



Deliverable Number: D 17.4

Deliverable Title: Report of an application of linked analysis and simulation

Delivery date: M48

Leading beneficiary:

Dissemination level:

Status: Complete

Authors: James Lord, Jamie Peck, Daniel O'Neill, Sean Giblin, Stephen Cottrell

Project number: 283883

Project acronym: NMI3-II

Project title: Integrated Infrastructure Initiative for Neutron Scattering and Muon Spectroscopy

Starting date: 1st of February 2012

Duration: 48 months

Call identifier: FP7-Infrastructures-2010

Funding scheme: Combination of CP & CSA – Integrating Activities

Linked Analysis and Simulation: An Overview

This report represents the conclusion of work carried out during this project considering the benefit of linking simulation methods with existing analysis codes. The focus of this deliverable is to report on three examples, selected from those discussed in the report submitted as Deliverable 17.3, which have been developed to illustrate the benefit of making this link.

For the first example, the FORTRAN code associated with the Quantum package has been refactored as Python subroutines that can be executed within the Mantid analysis framework. Execution under Mantid enhances functionality, providing the user with a seamless interface for reduction, analysis and interpretation. A number of examples have been developed to illustrate the scope and flexibility of the codes, and the report includes details to help setup and start using the package.

The second example reports on the development of Python codes for calculating the dipolar fields associated with both electronic and nuclear spin systems present in systems under study. An understanding of the internal fields is important for determining candidate muon sites in these systems, knowledge that is essential if a detailed understanding of the system is to be obtained from the μ SR measurements. Example applications are reported, and limitations of the present subroutines discussed. It's anticipated that development of these methods will continue under the EU SINE2020 project, with the intention of incorporating the subroutines within the Mantid framework.

The final example discusses potential benefits and limitations of linking *ab initio* Density Functional Theory (DFT) methods with existing μ SR data analysis codes. In this case, the focus of the work has been on establishing the efficacy of existing DFT packages for predicting parameters of hyperfine coupled systems. Work has tested the reliability of standard DFT codes by calculating parameters for an example system, and then continuing by exploring techniques for refining values obtained from these calculations. The possibility of using the technique as a predictive tool for the execution and analysis of Avoided Level Crossing μ SR measurements has been explored.

Stephen Cottrell
22 January, 2016

Integrating Quantum with Mantid

What is Quantum

QUANTUM is a program that uses the density matrix method for simulating the interaction between a series of spins, such as a muon and its neighbouring electrons and nuclei. It includes parameters such as dipolar, hyperfine and quadrupole interactions, external magnetic fields (static or RF) and fluctuations. Either single crystals with a defined orientation, or powder averages can be simulated.

Why run under Mantid

The original version of QUANTUM was written as a stand-alone FORTRAN program. It had basic plotting functionality but for publication quality graphs it was necessary to export the data into another package. Fitting of data also required the raw data to be prepared in a specific format.

The Mantid framework (see www.mantidproject.org for further information) provides all the missing functions such as the ability to load a wide variety of experimental data file formats, handling of data sets, and publication quality graphics. It can easily be extended using subroutines (known as Algorithms) written in C++ or Python.

Work carried out

QUANTUM has been rewritten in Python to be compatible with Mantid. As much of the work is carried out by library routines (IMSL library in FORTRAN, NumPy library in Python) the change to an interpreted language does not have much effect on the speed. NumPy and Mantid are better able to make use of multiple core processors.

Instead of a series of complex dialogs, the input parameters for the simulation are now stored in a Mantid table, which can be loaded and saved, edited by hand, or created by a script for more advanced simulations.

QUANTUM can run either as a simulation algorithm or a fit function, using the same model definition. As a fit function it can be used in the “Fit” stages of Mantid’s “Muon Analysis” or “Muon ALC” interfaces to directly fit user data.

Links and how to run the code

Mantid can be downloaded from: <http://download.mantidproject.org/>

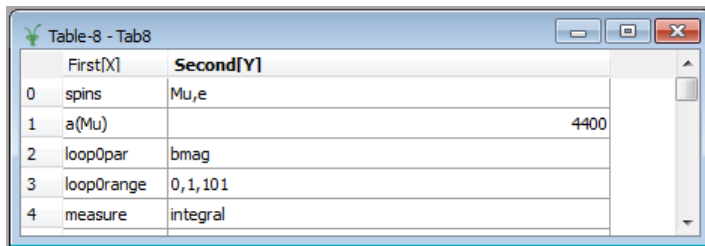
Once it has been installed, Quantum can be obtained from the Script Repository within Mantid, in section “Muon – Quantum”. Download all the files in the subfolders. These include the documentation.

Open Mantid’s Preferences dialog and add the Quantum subdirectory “Algorithms_Autoload” to Directories (Python scripts).

Restart Mantid so it loads the scripts. Quantum is now ready to be used.

Examples

A simple repolarisation curve



	First[X]	Second[Y]
0	spins	Mu,e
1	a(Mu)	4400
2	loop0par	bmag
3	loop0range	0,1,101
4	measure	integral

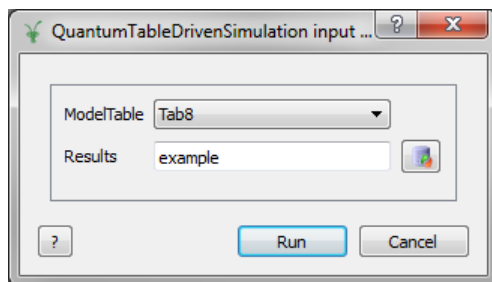
Line 0 defines the spins involved, and implicitly sets the gyromagnetic ratios.

Line 1 says we have an isotropic hyperfine coupling of 4400 MHz between the muon and the electron.

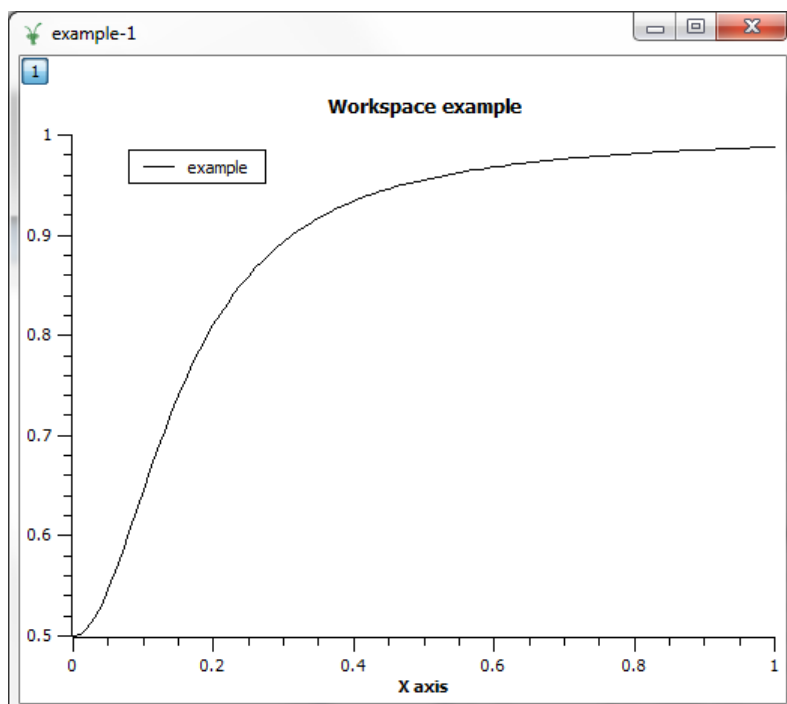
Lines 2 and 3 mean sweep the magnetic field from 0 to 1 Tesla with 101 points (100G steps).

Line 4 means take the integral asymmetry (by default the integration time is 0 to infinity, weighted by the muon lifetime).

Executing the algorithm...



The result (this example gives a workspace with 1 spectrum).



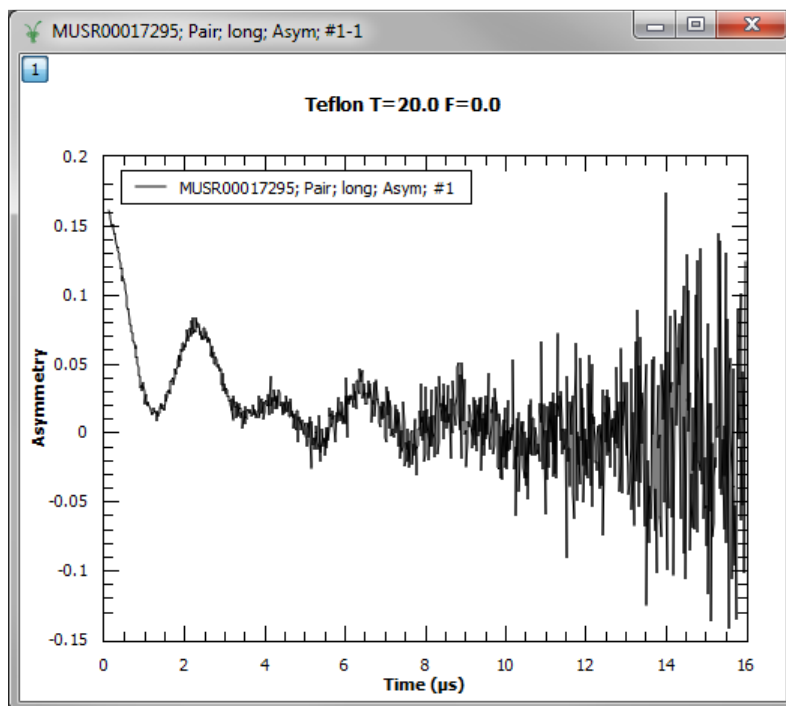
Fitting example: F-mu-F

Load the run in the Muon Interface

The screenshot shows the Muon Analysis software interface. The window title is "Muon Analysis". The interface is divided into several sections:

- Instrument:** A dropdown menu is set to "MUSR". Below it, "Time Zero" is 0.55 μs with a checked "From datafile" box. "First Good Data" is 0.11 μs with a checked "From datafile" box. "Dead Time Correction" is set to "From Data File". A description reads: "64 detector spectrometer, main field longitudinal to muon polarisation".
- Data Files:** A "Load current run" button is next to a text field containing "00017295". A "Browse" button and navigation arrows are also present.
- Detector Grouping:** "Group / Group Pair" is set to "long". "Alpha" is set to 1. "Data collected in 1 periods. Plot/analyse period:" has a dropdown set to "1", a "-" button, and a "None" dropdown.
- Plot Data:** "Plot type" is set to "Asymmetry". A "Plot" button is visible.
- Run Information:** A text area displays the following details:
 - Run: 17295
 - Title: Teflon T=20.0 F=0.0
 - Comment: slits 20
 - Start: 2008-Apr-22 17:07:38
 - End: 2008-Apr-22 17:49:54
 - Good frames: 115829
 - Counts: 33.504 MEV
 - Average Temperature: 20.061779367438
 - Sample Temperature: 20.000000000000
 - Sample Magnetic Field: 0.000000000000

At the bottom, a status bar shows "? Connected: MUSR00017295; Pair; long; Asym; #1" and a "Manage Directories" button.



Define the model. You must call the table "Tab".

Code[Y]	Value[Y]
0 spins	Mu,F1,F2
1 r(Mu)	0,0,0
2 r(F1)	0,0,1.2
3 r(F2)	0,0,-1.2
4 lfuniform	50
5 bmag	0
6 measure	timespectra
7 fit0par	r(F1)[2];-r(F2)[2]
8 fit1par	relax(F1);relax(F2)
9 dynamic	1
10 relax(F1)	0.1
11 relax(F2)	0.1
12	
13	
14	

(You can run QuantumTableDrivenSimulation on this directly to check if it looks about right)

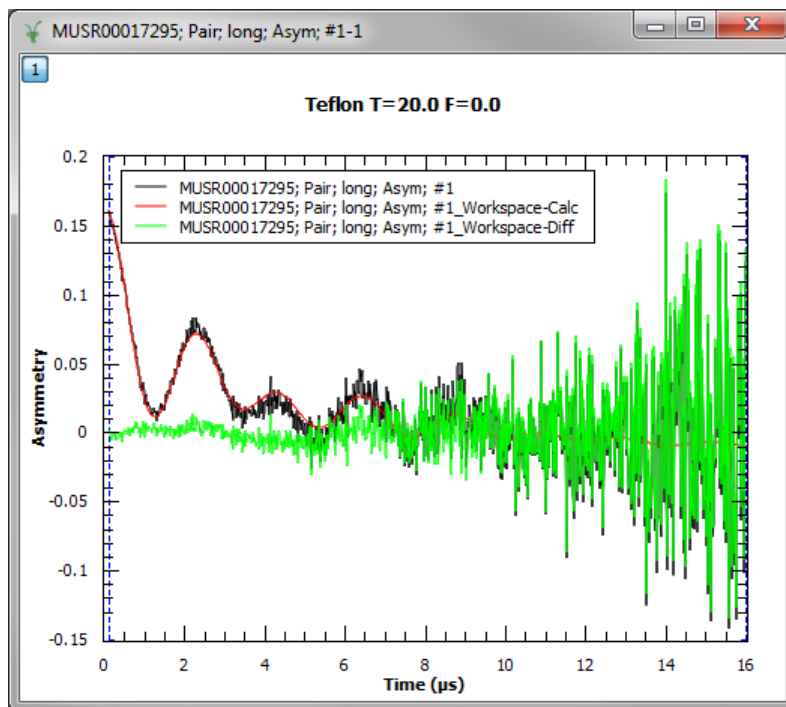
Select the Fit Function in the Muon interface. This model has 2 variables, fit0par is the Mu-F spacing and fit1par is the hop rate, so use the appropriate function. Give approximate starting values.

Fit Function

Fit Display Setup

Property	Value
Functions	
Type	CompositeFunction
NumDeriv	<input type="checkbox"/> False
f0-QuantumTableDrivenFunction2	
Type	QuantumTableDrivenFunction2
P0	1.200000
P1	0.100000
Scale	0.150000
Baseline	-0.050000
Data	
Workspace	MUSR00017295; Pair; long; Asym; #1
Workspace Index	0
Start (μs)	0.110000
End (μs)	16.000000
Settings	
Minimizer	Levenberg-Marquardt
Plot Difference	<input checked="" type="checkbox"/> True
Fit To Raw Data	<input type="checkbox"/> False
Show Parameter Errors	<input checked="" type="checkbox"/> True

Fit!



Fit parameters are displayed, with error bars:

Muon Analysis

Home | Grouping Options | Data Analysis | Results Table | Settings

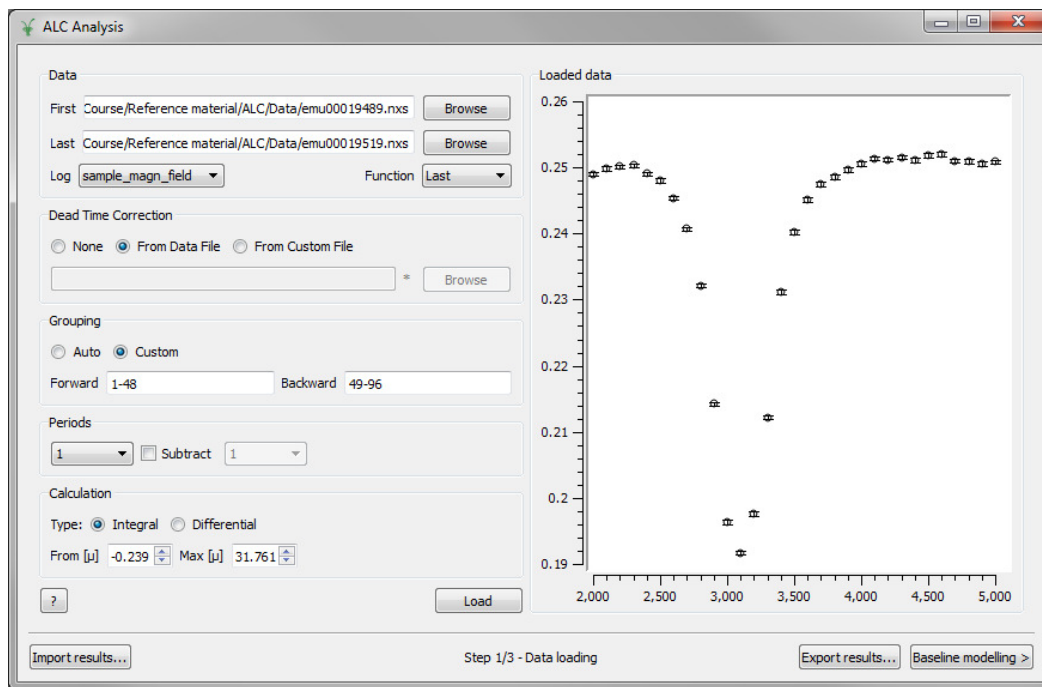
Fit Function (Chi-sq = 1.50879)

Fit | Display | Setup

Property	Value
Functions	
Type	CompositeFunction
NumDeriv	<input type="checkbox"/> False
f0-QuantumTableDrivenFunction2	
Type	QuantumTableDrivenFunction2
P0	1.227106 (0.000712)
P1	0.214425 (0.003034)
Scale	0.180639 (0.000775)
Baseline	-0.016989 (0.000429)
Data	
Workspace	MUSR00017295; Pair; long; Asym; #1
Workspace Index	0
Start (µs)	0.110000
End (µs)	16.000000
Settings	
Minimizer	Levenberg-Marquardt
Plot Difference	<input checked="" type="checkbox"/> True
Fit To Raw Data	<input type="checkbox"/> False
Show Parameter Errors	<input checked="" type="checkbox"/> True

Fitting example 2 - ALC

Load some data:



You may need to use the Background modelling, but it is not necessary for the baseline to be at 0.0.

Set up the Table:

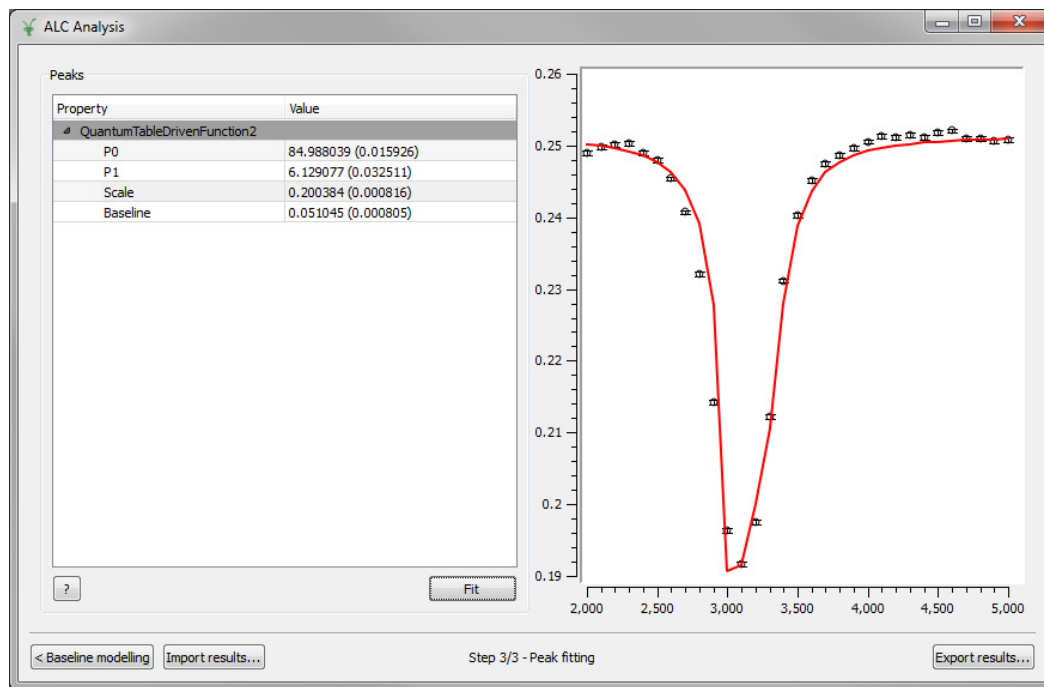
The screenshot shows a table configuration window titled "Table-1 - Tab". The table has two columns: "Code[Y]" and "Value[Y1]".

Code[Y]	Value[Y1]
0	spins
1	a(Mu)
2	lfuniform
3	measure
4	fit0par
5	fit1par
6	loop0par
7	bmagGauss
8	loop0range

Additional values are shown to the right of the table:

- lfuniform: 50
- measure: integral
- fit0par: a(Mu)[0]
- fit1par: a(Mu)[1]
- loop0par: bmagGauss
- bmagGauss: 2000
- loop0range: 2000,5000,31

Use the function:



What Can a Muon Tell Us About The Behaviour of Magnetic Systems?

Daniel O'Neill

School of Physics and Astronomy

University of Cardiff

May 2015

Abstract

As a way of considering the behaviour of magnetic systems, this project was designed to use computer modelling to replicate the results from μSR experiments. The premise was to investigate the local magnetic fields within crystals and to discover what these fields can tell us about magnetic systems. Existing code could be used to investigate fields within systems with ordered magnetic moments, the project was to expand and adapt this code to create computer modelling that could then be used to work within unordered systems.

The new code was first used to investigate CeInPt₄. The code was successful in reproducing the pattern of distribution of precession frequencies that were originally found using existing theoretical methods. However, the values produced using the new code were consistently greater than the values obtained either by using experimental or by these theoretical methods. I believe that this is most likely due to screening effects, which my model does not take into account.

The program was also used to investigate UCoGe in both the ferromagnetic and paramagnetic phases. The paramagnetic phase produced similar results to those obtained using CeInPt₄, once again with the values produced being significantly higher using the new coding. As before, I believe this to be a screening effect. In the ferromagnetic phase, contrary to this, the results predicted by the code were significantly lower than those found experimentally. The reasoning for this is because UCoGe, as well as having local, both spin and orbital, moments, has significant itinerant moments. The code is unable to take this into account at present leading to the discrepancy between theoretical and experimental results.

Contents

Introduction	12
Experimental Method	16
Results	19
CeInPt ₄	19
UCoGe.....	23
Discussion	28
CeInPt ₄	28
UCoGe.....	28
Conclusion	30
Bibliography	31

Introduction

This project investigates the effect of localised magnetic moments and their corresponding effect on the local magnetic field inside a material. This will be done by using code; theoretically reproducing the experimental results obtained using the technique μSR . All particles with spin have a magnetic moment that is generated by this spin, which means that in any sample there is a moment on each electron and each proton and neutron. These two nucleons sum to form the moment on the nucleus. The moments on the electrons are much higher than the nuclear components; however, this electron moment can fluctuate very rapidly. In some materials, below a certain temperature, these moments stop changing and this forms an ordered state. Two such states that are important for this project are superconductivity and ferromagnetism.

Superconductivity is a state where the resistance of a material falls to zero. The BCS theory (the Bardeen Cooper Schrieffer theory) explains how this can happen, whereby the electrons inside the material form Cooper pairs i.e. two electrons with opposite spins. This occurs because as an electron moves through the lattice it causes the lattice to change shape, attracting the lattice slightly towards the electron. This change in shape causes a slight, albeit temporary, build in charge that attracts another electron to the site. This attraction causes the electrons to be weakly bound to one another forming these pairs. The pairs form quasi-particles, mediated and controlled by phonon interactions. These quasi-particles have integer spin, as opposed to electrons, which are fermions with half integer spin. This allows them to condense into a Bose-Einstein condensate, as they no longer obey the Pauli's exclusion principle. A band gap is formed as these pairs occupy a lower energy state than other electrons in the crystal; this gap stops the collisions that lead to resistance that causes the material to become superconducting. [1]

Ferromagnetism is a different ordered state where the magnetic moments have the same orientation. This alignment causes an internal field, which in turn causes the alignment. This system can only exist when the temperature is below a given temperature that is particular for that material; this is called the Curie temperature. Above this temperature, thermal fluctuations destroy this ordering causing the material to return to a paramagnetic state where once again the moments on the electrons are not ordered. [2]

These two states would appear to be unable to co-exist because ferromagnetism requires the moments to be aligned with each other whereas superconductivity requires pairs of electrons with opposite spin. However, compounds have recently been discovered that are both ferromagnetic and superconducting simultaneously, such as UGe_2 (under pressure), $URhGe$ and $UCoGe$, [3] the last of which I will look at in more detail in this report. The co-existence is believed to be possible due to spin-triplet states. These are so called because there are 3 quantum states where S (the system spin) = 1 whereas there is only one state where $S = 0$ i.e. singlet electron

What can a Muon tell us about the behaviour of magnetic systems?

pairs, which are the pairs used for conventional superconductivity. These triplet states still allow for the integer spin needed for superconductivity whilst also allowing ferromagnetism to exist with all the moments on the electrons being aligned. It is even believed that this mechanism is mediated by the ferromagnetic fluctuations rather than phonons mediated as predicted by BSC theory for traditional superconductors. Superconductivity not mediated by phonons could be of great use in the ongoing search for new high temperature superconductors. The Curie temperature of UCoGe is 3K and becomes superconducting as well at $T_{sc} = 0.8K$

Muon SR or μSR is an experimental technique that is used to investigate the internal magnetic structure of materials. This technique uses the spin properties of muons to probe the local magnetic fields within a crystal, and with that calculate the moments within the crystal. The first part of the technique is to accelerate protons inside a particle accelerator to 800MeV [4] then fire them at a graphite target to produce pions. These pions have a half-life of 26ns and therefore decay rapidly. One of the products of the decay process is positively charged muons. Due to conservation of momentum, the muons produced are 100% spin polarised with their spin in the direction of their momentum. Next, using powerful magnets these muons are focused into a beam and aimed at the target material. Muons have a half-life of 2197ns, which allows them to reach the sample before decaying; this sample is sat between two detectors set up to detect the decay products of these muons. The muons then decay into positrons, which can be detected; the positrons momentum is preferentially in the direction of the muons spin so that in zero fields, the muons would decay without their spin changing and most of the positrons would be detected in the forwards detector. When the muon feels a field, however, this causes the spin to precess, rotating around the direction of that field at a frequency proportional to the magnitude of the field. This results in different count rates on the different detectors and the asymmetry of these rates can then be plotted.

Inside any material there are a large number of different local fields caused by the magnetic moments on the different particles inside the crystal. In a sample with ordered moments on the electrons, such as a superconductor, ferromagnet or antiferromagnet, the muons find sites in the crystal that are favourable and the field they feel at these sites produce a precession frequency that can be detected. Figure 1 shows the asymmetry of the numbers of positrons detected between the forward and back detector in a constant transverse field. At the start, the asymmetry is 1 as all the positrons detected are those which are detected on the forward detector since the muons have not had time to precess yet. As the time progresses the asymmetry moves toward -1 where all the positrons are then detected by the rear detector, and then back again as the spin of the muons precesses round the direction of the field.

What can a Muon tell us about the behaviour of magnetic systems?

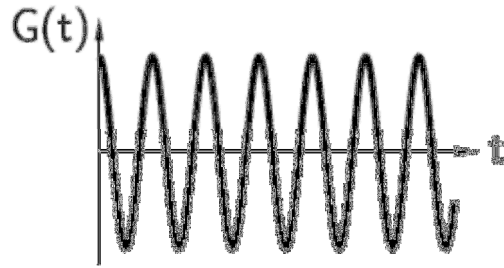


Figure 1 - plot of asymmetry of positrons detected against time in a constant longitudinal field [5]

The moments on the nucleus are much smaller than the electronic moments, meaning in the ordered phase they are negligible, of the order of the Nuclear magneton ($\mu_N = 5.05 \times 10^{-27} \text{ J/T}$) as opposed to the electronic moment of the order of the Bohr magneton ($\mu_B = 9.27 \times 10^{-24} \text{ J/T}$). However in the paramagnetic state above the critical temperature the moment on the electrons are oscillating at a frequency that is too fast for the muons to feel their effect on the field, i.e. the muon cannot process as fast as the field is changing. As a consequence, the moments on the nucleus can be measured. Since the moments on the nucleus are randomly orientated and since they are comprised by the sum of the moments on the protons and neutrons, they can vary between different isotopes of the same element., As a result, the muons in a position in one unit cell might not feel the same field as a muon in the same position in the next unit cell because the magnitude and direction of the moments contributing to the field may be different. Each muon produces an oscillating asymmetry as with the ordered phase, each with a frequency based on the field that muon processed around. The sum of these oscillations produces a curve called a Kubo-Toyabe, see Figure 2.

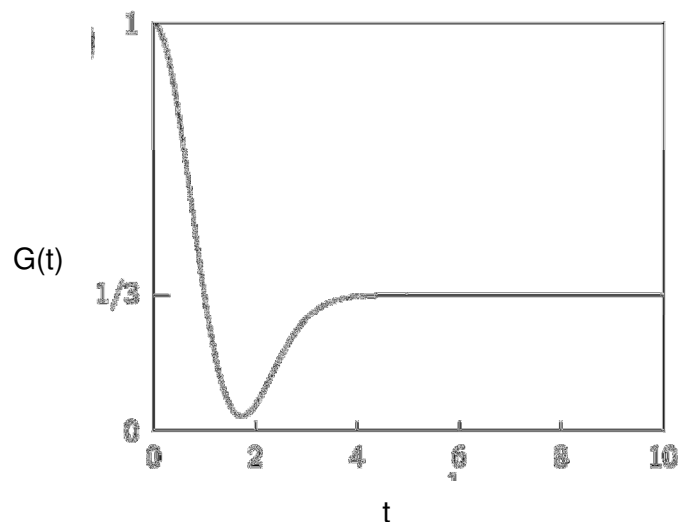


Figure 2 - Idealised Kubo-Toyabe relaxation function With asymmetry plotted against time [5]

What can a Muon tell us about the behaviour of magnetic systems?

The graph in Figure 2 is produced because each muon produces a sinusoidal wave starting at 1 when the time is equal to 0, of the form of equation 1. The value for θ is averaged over all directions because the direction is random, and this averaging gives equation 2. Each wave feels a slightly different field and therefore are slightly out of phase with one another, as shown in Figure 3. For each differing frequencies, therefore, as they are summed they form a graph that can be seen in Figure 2. The reason the graph settles at a third rather than 0 is because with a randomly orientated field a third of the incoming muons will find sites where the field aligns with the spin. Consequently, there is no asymmetry that can be detected, as the precession does not reach the rear detector.

$$\cos^2 \theta + \sin^2 \theta \cos \gamma_{\mu} B t \quad \text{Equation (1) [5]}$$

$$\frac{1}{3} + \frac{2}{3} \cos \gamma_{\mu} B t \quad \text{Equation (2) [5]}$$

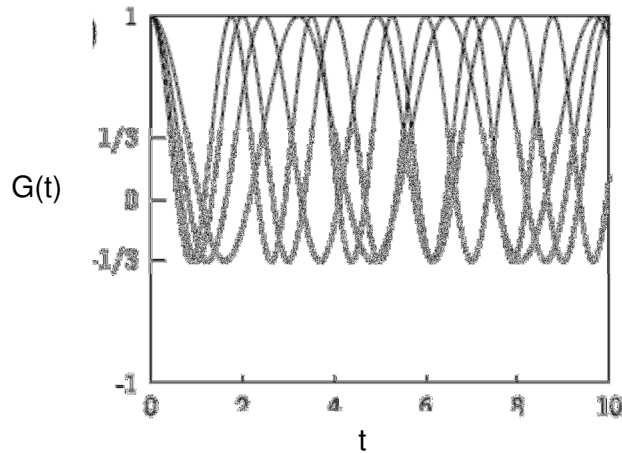


Figure 3 - asymmetry against time of many contributions to the precession frequency that sum to form the Kubo-Toyabe function

Summing the contributions of equation 2 gives the Kubo-Toyabe function. this has an equation of:

$$\frac{1}{3} + \frac{2}{3} (1 - \sigma^2 t^2) \exp\left(-\frac{\sigma^2 t^2}{2}\right) \quad \text{Equation (3)[3]}$$

Where σ is the nuclear depolarisation rate and $\sigma = \gamma_{\mu} B$ where γ_{μ} is the gyromagnetic ratio of the muon and B is the local field.

Experimental Method

The project commenced with program written in code produced by Andrew Steele as a PhD project [6]. The code was written using python to calculate the local field and, therefore, the precession frequency of an ordered system below the critical temperature. The code requires user inputs to define the crystal, the space group, the lattice vectors and angles. It also requires inputs about the atoms: their positions in the unit cell and their charge and, finally, inputs about the magnetic properties within the crystal, i.e. the moments and the propagation vector (a measure of how many cells are required for the ordering to repeat) to be assigned to each atom with a moment. From this the program can create a crystallographic unit cell and a magnetic unit cell; for example, Manganese Oxide can be seen in Figure 4(a) and 4(b).

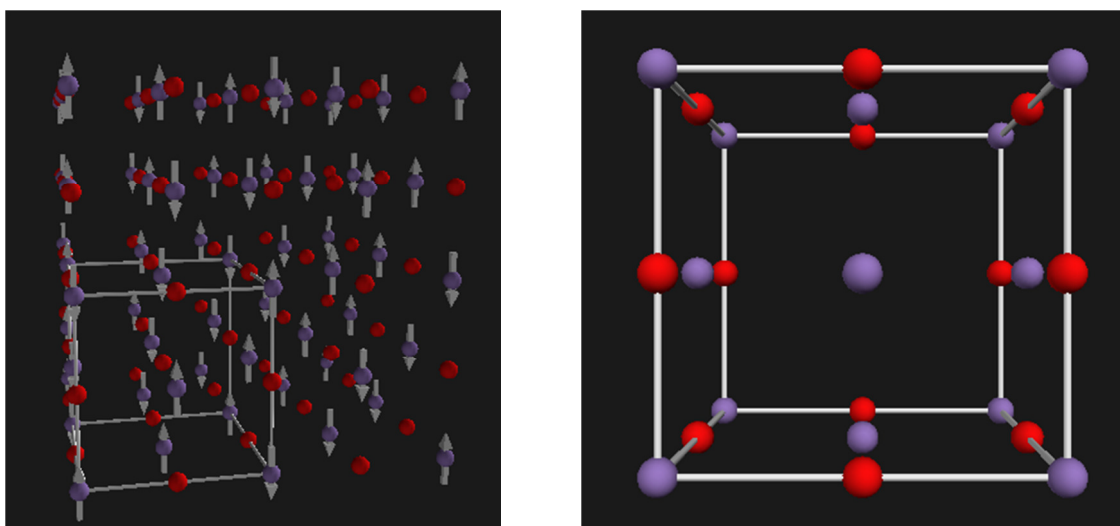


Figure 4(a) - magnetic unit cell and Figure 4(b) - crystallographic unit cell of MnO

The program then uses dipole calculations to work out the field at each point for a crystal of a given size. It does this by, at each point, working out the field at that point caused by each magnetic moment and summing them. The code's output are files containing vectors of the field with the frequency and each position defined inside the portion of crystal being investigated. The program can then plot this data on the magnetic unit cell shown in Figure 4. Figure 5 shows the magnetic unit cell with the possible sites. The user inputs a range of precession frequencies with the sites within the crystal that are at those frequencies being shown as results. In consequence, if the experimental value for the precession frequency is inputted, possible muon sites will be shown; for example MnO has a frequency of 256MHz so the range of 235 to 275MHz was entered, as shown in Figure 5.

What can a Muon tell us about the behaviour of magnetic systems?

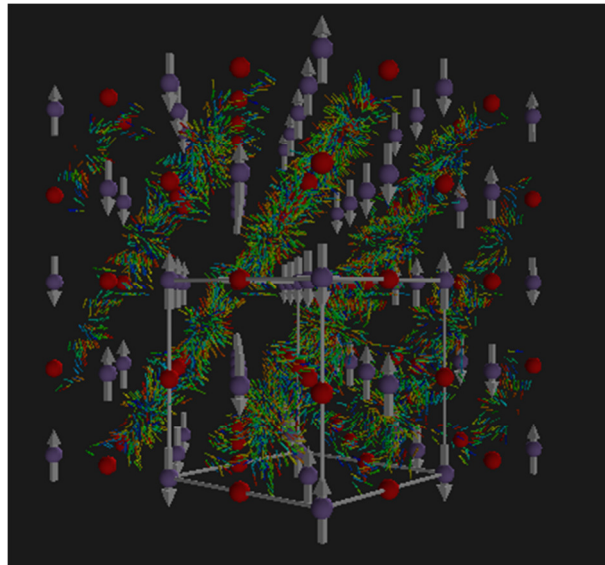


Figure 5 - possible sites of muons in MnO

The changes that were made to the original code now allow it to run the same calculations on crystals, however in the paramagnetic phase, where the nuclear spin dominates. There were three key changes to be made to the code to allow this, which were;

- allowing the input of isotopes of the atoms,
- randomly orientating the moments as opposed to only having user defined magnitudes,
- running large numbers of calculations on the part of the crystal being investigated, with random isotopes and directions, and then averaging the results of the fields.

The first of these changes to the code, the input of isotopes, was important because the magnitude of the moment on the nucleus is the sum of the moments on the protons and the neutrons and therefore varies with different isotopes, since the number of neutrons change. This is one of the reasons that the field felt by the muon in its site can vary from unit cell to unit cell. This addition to the program therefore involved a user input of the different isotopes. Of necessity, this required the inclusion of information on the element, the atomic mass, the abundance and the nuclear moment for each isotope, for each atom in the crystal. The change in the program then, when building the virtual crystal, assigns a range of values all within the range of 0 and 1 for each isotope then, when placing an atom, generates a random number between 0 and 1 and uses the isotope whose range the random number falls within. This gives a random selection of isotopes in the correct abundances.

The second change to the code involved the random orientation of each moment. This also has an effect as it changes the direction of the contribution to the field at

What can a Muon tell us about the behaviour of magnetic systems?

the sites and therefore when the magnitude of all the contributions are added together the sums could have a very different magnitude and direction each time, which changes the precession frequency of the muon. The original code needed a repeating pattern and therefore a magnetic propagation vector, k , was used. The moment was then multiplied by $e^{2\pi i k \cdot T}$, where T is the integer number of the cell. This allowed the moments to repeat after a given number of unit cells; for example, if the system was ferromagnetic the k vector would be $(1,1,1)$ so it would repeat in the next unit cell in all three directions but if, as in the example above, the system was antiferromagnetic the k vector would be $(\frac{1}{2}, \frac{1}{2}, \frac{1}{2})$ and it would take two unit cells to repeat. Subsequent changes to the code completely changes this and instead, using spherical polar coordinates, randomly generated a θ and ϕ value between 0 and 2π and 0 and π respectively, then calculated a new vector for the moment by transforming it back into Cartesian coordinates. This allowed a random direction without changing the magnitude of the moments.

The final change to the code was to average a large number of runs, this was important because otherwise, with only one run, the calculation would be based on each site within only one unit cell in the crystal. The average over many runs gives the static local field, averaging the precession frequency making it independent of the direction of the spins in the crystal. This was done by simply adding to the program a 'for' loop in the code at the point that the local field is calculated. The code requests a general name for the files, the number of runs to be averaged over, and the size of crystal to be looked at in unit cells. At the end of the run two final files are created, one with the mean of the field and precession frequency at every point in the crystal, the other with the maximum values. Whether the frequencies within the crystal have converged can be tested by taking the average frequency at any point in the crystal for each run up to the total. This value will randomly fluctuate at first but settles to a value after a large enough number of runs.

In addition to these changes to the original code, a separate code to perform the necessary analysis on the output files was written. This additional code took the final mean or maximum files and produced a histogram of the frequencies with the experimental values plotted on it. The code also produced images of the precession frequency in any plane in the crystal with contours plotted of the experimental value. The final graph the code produces is a Kubo-Toyabe by putting the experimental value into equation 3 to reproduce the data obtained.

Results

CeInPt₄

CeInPt₄ was the first crystal that was used to test the new adaptations made to the code. The crystal has a space group of $F\bar{4}3m$ (No. 216)[7] which is a cubic structure and that all three lattice parameters are equal and all three of the angles equate to 90° . For this crystal $a = b = c = 7.6129\text{\AA}$ [7]. To initially test the program a run was carried out whereby only the most abundant isotope of each element was used, these being ^{140}Ce , ^{115}In , and ^{195}Pt which have nuclear moments of 0, 5.5408, and 0.60950 respectively[8]. To further simplify this initial run the Pt moment was considered negligible and, therefore, also ignored. The program was run using these parameters and the average over 500 runs was taken and compared to the experimental results. The number of runs was set at 500 runs, a figure which was used because the frequency was shown to converge and settle to a static field for this value, as Figure 6 shows.

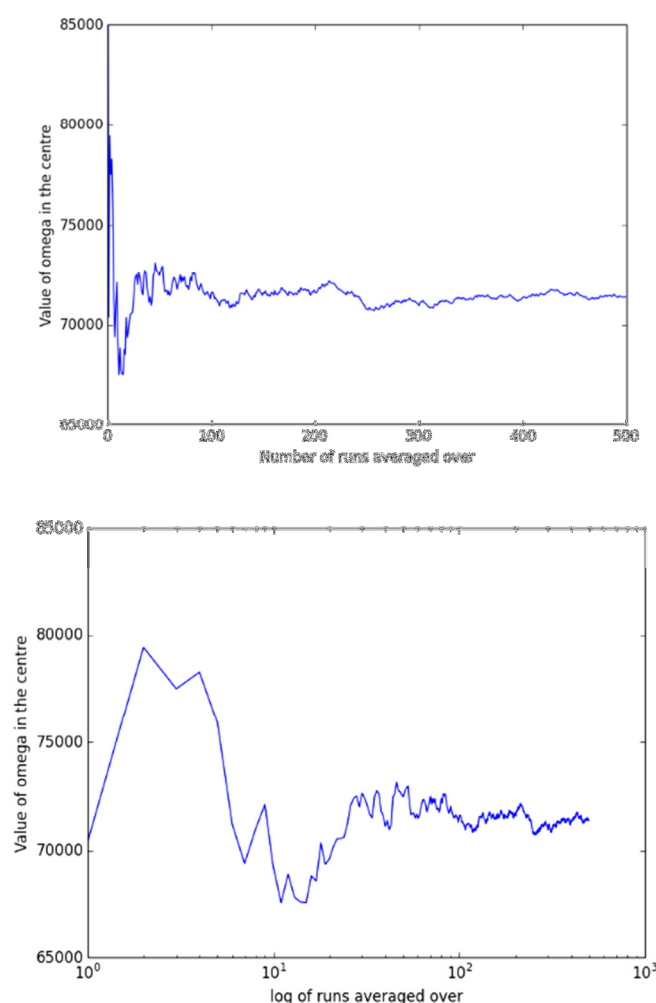


Figure 6 - plot of the average frequency, in Hz, from the (0.5,0.25,0.25) position against (a) the number of runs complete and (b) the log of the number of runs completed

What can a Muon tell us about the behaviour of magnetic systems?

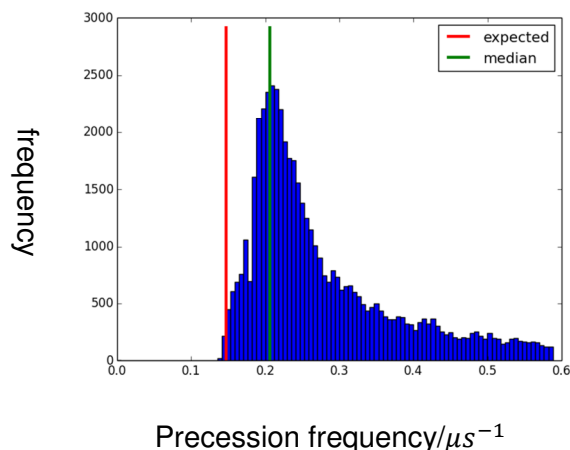


Figure 7 - histogram of frequencies, in μs^{-1} , within the unit cell where the red line is the experimental value

Experimentally the nuclear depolarisation rate was found to be $\sigma = 0.147\mu s^{-1}$ [7] which has been plotted on the histogram of frequencies in Figure 7.

From the values for the median and the experimental value two Kubo-Toyabe function can be plotted, using equation 3. These are plotted in Figure 8 and show that there would be a slight but noticeable difference between the experimental result and the result obtained using the program

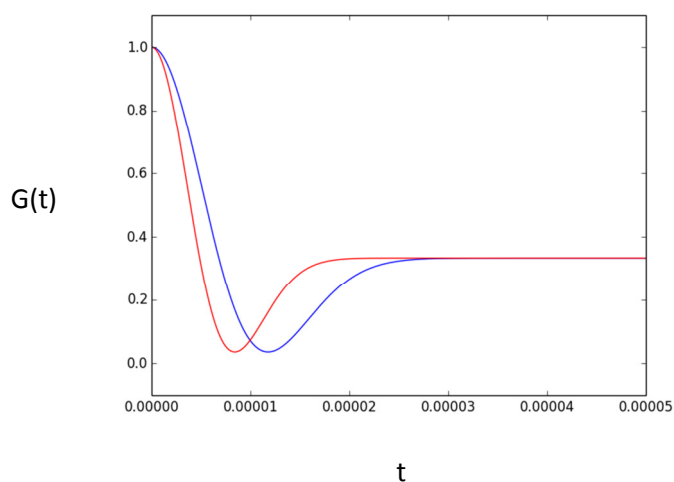


Figure 8 - Kubo-Toyabe functions of time, in s, against asymmetry using the experimental (blue) and average (red) values for the precession frequency

Calculations performed by A.D. Hillier et al. determined that the most probable muon sites were situated at (0.5, 0.5, 0.25) and equivalent sites [7] and calculated the frequency positions in the $x = 0.5$ plane as shown in Figure 9(a). Reproducing the same plane using the results obtained by the program can be shown in Figure 9(b),

What can a Muon tell us about the behaviour of magnetic systems?

i.e. the same distribution of frequencies but at higher values. This is also shown in the histogram of frequencies graph in Figure 7. This result was possibly due to other effects within the crystal that the program did not take into account, such as screening. Screening is where electrons between the moments and the sites shield the moment, reducing the local field at that site.

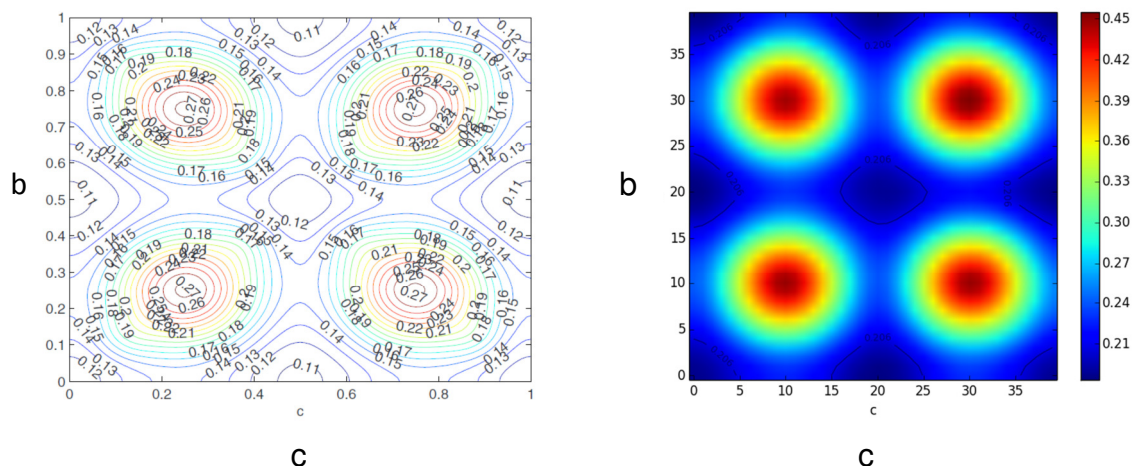


Figure 9(a) - contour plot of muon depolarisation rate in the $x=0.5$ plane by A.D. Hillier et al. [7]

Figure 9(b) - image of the $x=0.5$ plane from the program

This same calculation was repeated using a more complete view of CeInPt_4 , with all stable isotopes of the atoms being and used with all of their moments used. As discussed above, a random generator was used to choose which isotope sat on which site with a separate random generator being used to assign a direction as before. The isotopes and their moments are set out within Table 1 below.

Isotope	Relative Abundance	Nuclear Moment/ μ_N
^{136}Ce	0.00185	0
^{138}Ce	0.00251	0
^{140}Ce	0.88450	0
^{142}Ce	0.11114	0
^{113}In	0.04295	5.5289
^{115}In	0.95715	5.5408
^{190}Pt	0.00014	0
^{192}Pt	0.00782	0
^{194}Pt	0.32967	0
^{195}Pt	0.33832	0.60950
^{196}Pt	0.25242	0
^{198}Pt	0.07163	0

Table 1 – Stable isotopes, their abundances and their nuclear moments for Ce, In and Pt [8]

What can a Muon tell us about the behaviour of magnetic systems?

In the same manner as for the simpler example, the program was run with an average over 500 runs to allow the field to converge on to a stable value. The same analysis was performed on this more complex example as was initially used on the above-simplified model. Figure 10 below shows the histogram and the Kubo-Toyabe results of the runs including the isotopes. As can be seen, it is clear that there is no significant change in the values delivered from those seen in the earlier simple model. However, the peak of the distribution is more rounded and less defined making the median shift slightly from the value achieved in the simplified model.

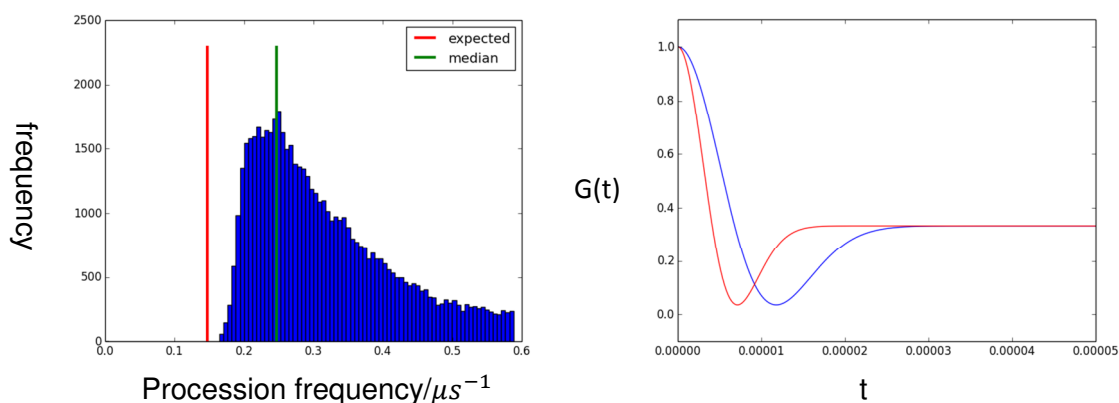


Figure 10a - histogram of the precession frequencies, in μs^{-1} , within a single unit cell of the complex model

Figure 10b – Kubo-Toyabe functions of time, in s, against asymmetry using the experimental (blue) and average (red) values for the precession frequency, calculated from the model with all isotopes included.

The biggest change seen between these results and those of the simplified model comes from the analysis of the $x=0.5$ plane, as shown in Figure 11 below. The changes to the inputs, predominantly the small moment a third of the Pt atoms, causes the changes seen, these extra moments contribute to the stretching or perhaps ellipsing of the circles at the (0.5,0.25,0.25), (0.5,0.25,0.75), (0.5,0.75,0.25), and (0.5,0.75,0.75) sites.

What can a Muon tell us about the behaviour of magnetic systems?

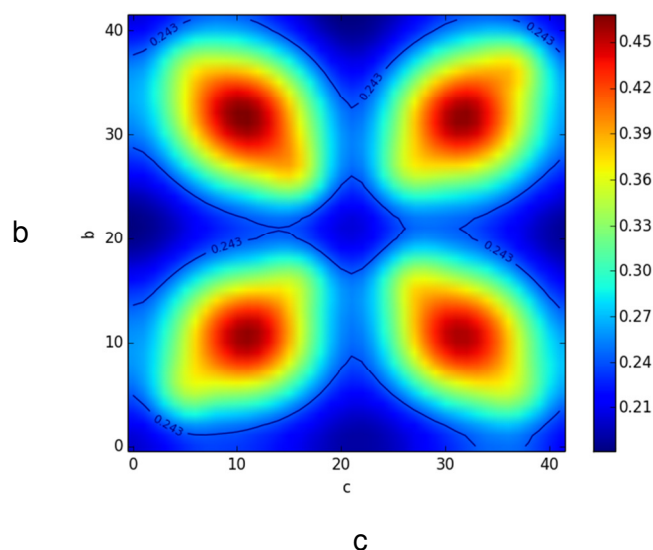


Figure 11 - image of the $x = 0.5$ plane of $CeInPt_4$ taking into account all the isotopes mentioned in Table 1

UCoGe

UCoGe is, as discussed above, a material that at 0.8K becomes both ferromagnetic and superconducting. It is a cubic crystal with a space group of Pnma [3] and with lattice vectors of $a = 6.852\text{\AA}$, $b = 4.208\text{\AA}$ and $c = 7.226\text{\AA}$ [9]. Like in $CeInPt_4$ the cubic structure means that all three angles are 90° . However, unlike with the first crystal a simplified crystal was not used initially and all the isotopes were used from the outset. The isotopes for Uranium, Cobalt and Germanium needed for the program can be seen in Table 2 below. As can clearly be seen the local field within the crystal is dominated by the moment on the ^{59}Co as there is only small moments on rare isotopes for the other two elements.

Isotope	Relative Abundance	Nuclear Moment / μ_N
^{234}U	0.0000552	0.0
^{235}U	0.00720051	-0.35
^{238}U	0.992745106	0.0
^{59}Co	1.0	4.627
^{70}Ge	0.2084	0
^{72}Ge	0.2754	0
^{73}Ge	0.0773	-0.8794669
^{74}Ge	0.3628	0
^{76}Ge	0.0761	0

Table 2 - isotopes, relative abundances and Nuclear Moments for Uranium, Cobalt and Germanium [8]

What can a Muon tell us about the behaviour of magnetic systems?

Once again the program was run 500 times to create a static field result as before. Similar analysis was applied to the results as to the earlier crystal of CeInPt₄. Figure 12 below shows the histogram of frequencies inside the unit cell with the experimental value, that was found to be $0.3\mu s^{-1}$ [3], plotted as well.

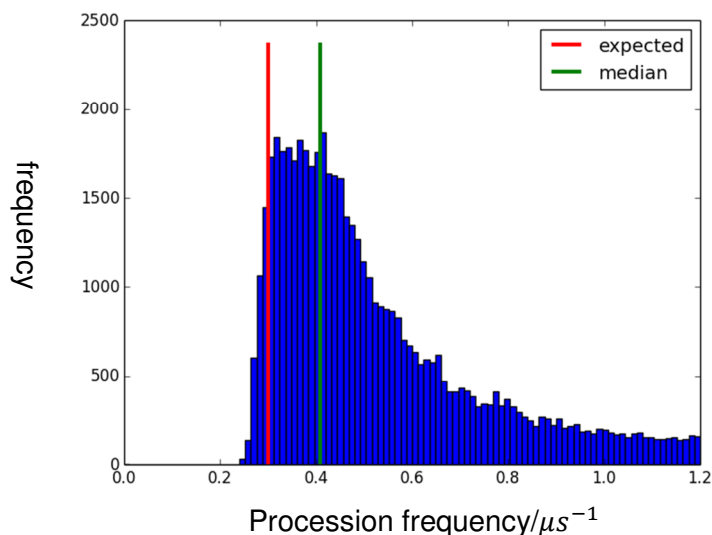


Figure 12 – histogram of precession frequencies, in μs^{-1} found within the unit cell of UCoGe

Like the CeInPt₄ example, when using all the isotopes, the peak of the histogram is quite flat affecting where the median is placed. The experimental result is also closer to the peak implying the possibility of less screening lowering the local field and therefore the precession frequencies at the sites within the crystal. Figure 13 shows this, as can be seen by the two Kubo-Toyabe functions being much closer to each other than the Kubo-Toyabe functions with the CeInPt₄.

What can a Muon tell us about the behaviour of magnetic systems?

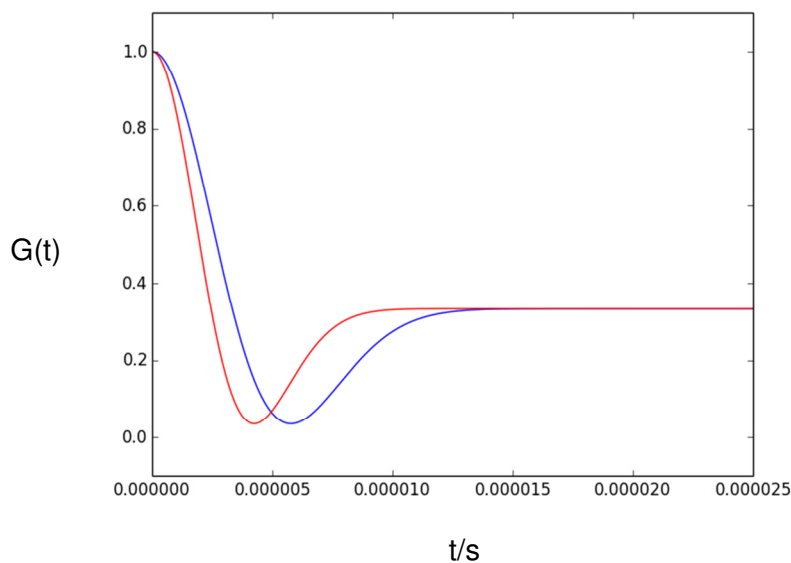


Figure 13 - Kubo-Toyabe functions of time, in s, against asymmetry using the experimental (blue) and average (red) values for the precession frequency, for UCoGe

It was determined by A.de Visser et al that the most probable muon sites are the 4a and 4b sites in the Wyckoff notation [3], the 4b sites corresponding to (0,0,0.5), (0.5,0,0), (0,0.5,0.5), and (0.5,0.5,0) in fractional coordinates and the 4a sites corresponding to (0,0,0), (0.5,0,0.5), (0,0.5,0), and (0.5,0.5,0.5). The plane that was chosen to be investigated was the $y=0.5$ plane as it contains several of these points. Figure 14 below is the image of this plane with a contour plotted for the value produced by the program.

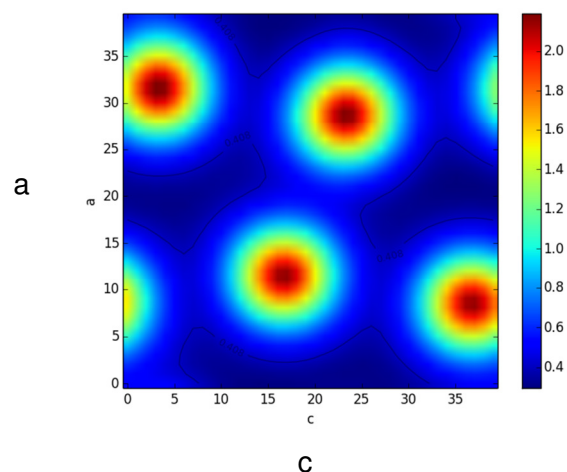


Figure 14 - image of the distribution of frequencies in the $y=0.5$ plane of UCoGe with contour plotted at the median value ($0.408\mu\text{s}^{-1}$)

What can a Muon tell us about the behaviour of magnetic systems?

The next experiment run was UCoGe with the original program using the moments from the ordered, ferromagnetic phases. This run used the same crystal structure discussed above however with different moments. The moments on each atom were experimentally calculated at 5T. The spin moment on the uranium was found to be $U_s = -0.30\mu_B$ and the orbital moment was found to be -1.3 times the size of the spin, ie, $U_l = -1.3 \times -0.30 = 0.39$. The spin moment of the Cobalt was found to be $Co_s = 0.06\mu_B$. [10]. The spin moments were calculated using Compton scattering; this is where the electron momentum density is measured by observing the scattering of high energy x-rays fired at the surface. The orbital moments are measured by comparing the spin moments to the bulk magnetisation. These moments were scaled to zero field by creating a ratio between the total moment in a 5T field, $0.16\mu_B$ [10], and the total moment in zero field, $0.043\mu_B$ [11]. This made it possible to produce zero field moments for the atoms, $U_s = 0.080625$, $U_l = 0.1048125$ and $Co_s = 0.016125$. These moments were inputted in the y-direction and the propagation vector for all the moments was 1,1,1 as all the moments were ferromagnetic and repeat each unit cell. Once again, the frequencies were plotted as a histogram with an experimental value of 1.972MHz [3], as shown in Figure 15. The experimental value here was much higher than the average value. This difference could be due to the fact that there is an itinerant moment within the crystal whereas the program was only designed to allow the input of local moments. This is discussed further later in this report

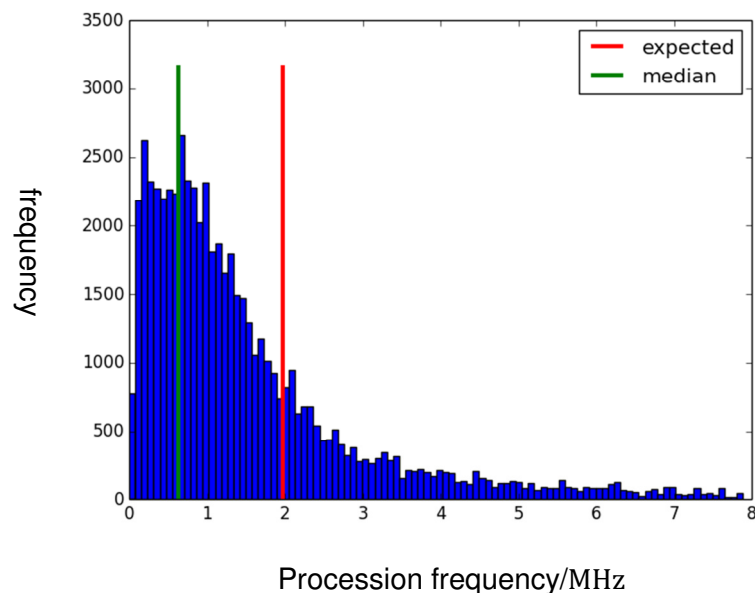


Figure 15 – histogram of precession frequencies, in MHz, within the unit cell of UCoGe

To compare these results to the nuclear component above the critical temperature the distribution in the $y=0.5$ plane was plotted, as shown in Figure 16 below. The two

What can a Muon tell us about the behaviour of magnetic systems?

contours on the plot are the experimental value and the average value from the histogram. The results obtained are discussed below.

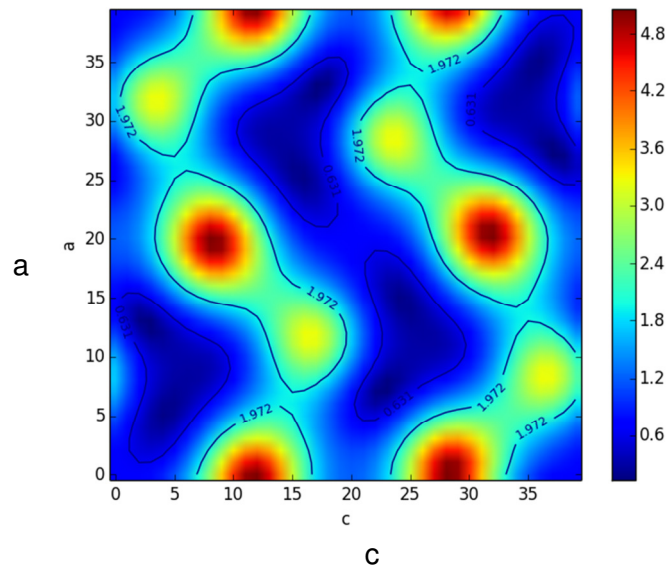


Figure 16 – image of the distribution of frequencies in the $y=0.5$ plane in $UCoGe$, with contours at the experimental value (1.972MHz) and the average value (0.631)

Discussion

CeInPt₄

As previously outlined, the values obtained in the simplified and more complex model for the local field and precession frequency were consistently higher than expected from the experimental results as is shown in the histograms in Figure 7 and Figure 10a. A possible cause for these differences could be as a result of electron screening i.e. the field felt at points in the crystal is reduced as the effects of the moments are screened by intervening electrons. This effect would reduce the field felt by the muon at a site within the crystal from the level that was predicted by the program to a lower value and, since the precession frequency is proportional to that field, this would also reduce. A way to test whether this effect is responsible for the difference in the results would be to test the program on a material with a very small degree of screening, i.e., an insulator. Although I briefly tested the coding with LiCoO₂ however this resulted in much more complexity to the program, something that could be taken forward at a later date. The time constraints of this project did not allow me to complete the more complicated analysis required for a non-cubic structure.

The shape of the distribution of the frequencies in the $x=0.5$ plane for the simplified crystal is the same as the shape of distribution predicted by A.D. Hillier et al, as seen in Figure 9a. However, the shape is different when the other isotopes and moments are added which suggests that the formula used in Hillier's paper to obtain the contour plot only used the moment on the most abundant atoms ignoring the small moment on some of the Pt atoms whilst also ignoring the isotopes that slightly changes the shape. This cannot be concluded with certainty as the screening has not been taken into account. Interpreting this effect could potentially become complicated with moments on multiple atoms as they each could be screened differently. It should be possible to improve the code so that the program can take screening into account and produce more accurate results.

UCoGe

As mentioned above the calculation was carried out both using the original program in the ferromagnetic phase with ordered moments and using the new program in the paramagnetic phase. The results from the paramagnetic phase, as with the results using CeInPt₄, are once again higher than the experimental value. This is most likely due to screening lowering the field felt at sites within the unit cell. There is a smaller difference with UCoGe than with the CeInPt₄ crystal, which may be due to a smaller amount of screening in the latter than in the first crystal.

In the ferromagnetic phase the $y=0.5$ plane looks very different from the paramagnetic phase. This is because in this ferromagnetic phase there are similar moments on both the Cobalt and Uranium atoms whereas in the paramagnetic

What can a Muon tell us about the behaviour of magnetic systems?

phase there is a significantly larger moment on the cobalt than any other atom. With the additional fact that the moments are significantly larger and all aligned in the ferromagnetic phase, it means that the field and therefore frequency is much higher than in the paramagnetic phase. These general differences in the phases were expected and as shown can be reproduced by the program however; as yet, it is not possible to reproduce the values at this point.

The experimental frequency in the ferromagnetic phase is a lot higher than the frequency which the program suggested, which is likely due to the fact that in addition to the local moments (both orbital and spin) within the crystal there are itinerant moments throughout the entire material. However, the program does not have the capability to take itinerant moments into account. Once again, going forward, it should be possible to add the ability to include itinerant into the code without too much difficulty allowing more accurate results to be reproduced

There is a third phase that this crystal can achieve, i.e. the ferromagnetic-superconducting phase. The experimental precession frequency rises significantly as it changed from the paramagnetic to ferromagnetic phase and then only drops slightly when into this third phase. This is due to a change in the moments on the atom as the phase changes. However, without introducing into the program a way to deal with both the screening in the paramagnetic phase and the itinerant moments in the ferromagnetic phase it is not possible to find the changes to the moments that cause these changes to the precession frequency.

This program was very much a first step in the process and as such can be considered successful. It can be seen to approach and follow experimental results closely for the more simple crystal structures and can, I believe, be adapted to more complex structures with relatively simple additions to the program, as mentioned above. These few steps will take the program forward and allow a much clearer look at the sites for UCoGe, possibly allowing a method of investigating the change in moments that lead to the crystal becoming a superconductor. It was the prospect of this particular aspect of Moments that inspired the investigation and this project in the first place.

Conclusion

This project was designed to use computer modelling to replicate the results from μSR experiments. The project aimed to adapt Andrew Steele's program. His original program was designed to investigate the internal local fields within a crystal using the moments on the atoms and converting these fields into the precession frequencies that muons would experience in these fields. The original code was designed to work within an ordered state. My project was to expand and adapt this code to create computer modelling that could then be used to work within unordered systems.

The adapted code was applied to $CeInPt_4$ in order to establish whether it could replicate the results obtained through μSR experimentation. The results of the experiments demonstrated that the shape of the distribution can indeed be replicated. However, the values that were produced were higher than expected, possibly due to a screening effect that would lower the frequency throughout.

When applied to $UCoGe$, in the paramagnetic phase, the fields that the program produced were once again too high which could be due to screening. However, in the ferromagnetic phase, when using the original program, the fields produced by the program were too low. This is likely to be due to the inability to add itinerant moments

Bibliography

- [1] – C. Kittel (1963) *Quantum Theory of Solids* London; John Wiley & sons Inc
- [2] – S. Blundell (2001) *Magnetism in Condensed Matter* Oxford; Oxford University press
- [3] – A. de Viser, N.T. Huy, A. Gasparini, D.E. de Nijs, D. Andreica, C. Baines, and A. Amato (2009) 'Muon spin rotation and relaxation in the superconducting ferromagnet UCoGe' *Physics Review Letters* 102, 167003
- [4] – <http://www.isis.stfc.ac.uk/groups/muons/muon-training-school/2014-hillier-muon-instrumentation14910.pdf> Last Accessed 10/05/2015
- [5] – S.J. Blundell (1999) 'Spin-polarized muons in condensed matter physics' *Contemporary Physics* 40 Issue 3
- [6] – <http://andrewsteele.co.uk/physics/mmcalt/docs/install> last accessed 10/05/2015
- [7] – A. D. Hillier, D. T. Adroja, S. R. Giblin, and W. Kockelmann (2007) 'Understanding the heavy fermion behaviour in CeInPt4' *Physical Review B* 76, 174439
- [8] – <http://www.webelements.com/> Last accessed 10/05/2015
- [9] – M. Samsel-Czekala, S. Elgazzar, P.M. Oppeneer, E. Talik, W. Walerczyk, and R. Troc (2010) 'The electronic Structure of UCoGe by *ab initio* calculations and XPS experiment' *Journal of Physics: Condensed Matter* Vol 22 015503
- [10] – M.W. Butchers, J.A. Duffy, J.W. Taylor, S.R. Giblin, S.B. Dugdale, C. Stock, E.D. Bauer, and C. Paulsen 'Determination of spin and orbital magnetization in the ferromagnetic superconductor UCoGe' (*unpublished*)
- [11] – C. Paulsen, D.J. Hykel, K. Hasselbach, and D. Aoki (2012) 'Observation of the Meissner-Oschensfeld Effect and the Absence of the Meissner State in UCoGe' *Physical Review Letters* 109, 237001

Simulating hyperfine coupling constants of muoniated radicals using density functional theory calculations

Jamie Peck, Francis Pratt and Stephen Cottrell

Abstract

In this work we consider potential benefits, and limitations of linking *ab initio* Density Functional Theory (DFT) methods with existing μ SR data analysis codes. This is motivated by the desire to provide users of the μ SR technique with additional tools to help them better understand and interpret their data. The DFT method may be considered as complementary to the μ SR technique. It is essential for interpreting muonium chemistry type experiments, where it provides the experimenter with an indication of the appropriate field regions where resonances are likely to be found, and can also help assign resonances to nuclei and identify the muonium binding sites during data analysis. A link between data analysis and DFT simulation codes is therefore likely to be highly beneficial in making efficient use of beamtime.

The support for this work provided by the European Commission under the 7th Framework Programme through the 'Research Infrastructures' action of the 'Capacities' Program, NMI3-II Grant Number 283883, is gratefully acknowledged.

Table of Contents

1	Introduction.....	34
1.1	Quantum mechanical model.....	35
1.2	Basis sets.....	36
1.3	Practical considerations.....	37
1.4	μ SR theoretical background.....	38
1.4.1	Transverse field- μ SR	40
1.4.2	Avoided level crossing- μ SR	40
2	Developing a model for the muoniated cyclohexadienyl radical.....	42
2.1	Evaluating popular DFT methods	42
2.2	Considering the isotope effect.....	45
2.3	Vibrational averaging.....	46
2.3.1	C- μ stretching vibration	48
2.3.2	C- μ bending vibrations	51
2.3.3	Averaging vibrational contributions for comparison with experimental data.....	53
2.3.4	Nuclear couplings	55
3	Conclusions.....	58
3.1	Outcome of the study of the cyclohexadienyl radical.....	58
3.2	Recommendations for further work	58
	Note Added in Proof	60
4	Appendix.....	61
5	References.....	62

1 Introduction

This document investigates the feasibility of linking DFT codes with existing μ SR data analysis software, providing a resource for the “inexperienced” user to predict isotropic hyperfine coupling constants (hfcc) in simple organic systems. The term “inexperienced” implies that the user has minimal knowledge of the strengths and weaknesses of the methodology used in the DFT technique.

Ideally, the algorithm would work something like this: the user would select an appropriate/reliable functional and basis set (model chemistry) for their structure(s) (there might be help in the form of an ‘expert system’ to define the problem) and run the simulation to obtain the muon and nuclear hfcc with minimum user input. However, before we can consider DFT methods as a ‘black box’ for obtaining this type of information, we need to understand both the limitations on the accuracy of the results (and how this might be improved), and the impact on the results that an inappropriately defined problem might have. This work seeks to understand these limitations by testing the methodology on a simple, well characterised, prototype system.

Due to its simplicity, and the availability of muon and proton hfcc temperature dependence data, the cyclohexadienyl muoniated radical was chosen as a prototype system. We begin by evaluating some choice model chemistries and methodologies, and using these to predict isotropic hfcc, and move on to develop a methodology for zero-point energy (ZPE) correction.

1.1 Quantum mechanical model

DFT can be used to investigate solid-state systems and atomic/molecular systems. Here, we are interested in the latter, and the best comprehensive review of DFT for this context is by Parr and Yang, in ‘Density functional theory for atoms and molecules’ [1]. However, Koch’s ‘A chemist’s guide to density functional theory’ offers an arguably more palatable overview (from a chemists perspective) of the technique [2]. Here, we offer only a very brief introduction, and readers are urged to consult the above texts for a more detailed account of the technique.

DFT is based on two theorems proved by Hohenberg and Kohn in the mid 1960’s [3,4]. They state that a description of molecular system is provided by its electron density, $\rho(r)$ and as such, all properties of the ground state system are functionals of $\rho(r)$. The implications of these theorems reduce the problem of calculating the electronic wave function in $3N$ dimensional space (which is the case in Hartree Fock, Configuration Interaction, and perturbation theory calculations) to calculating the electron density in 3D space using a single set of atomic coordinates. The Kohn-Sham Hamiltonian is expressed by:

$$\hat{H}_{KS} = -\frac{1}{2}\nabla^2 + v_H + v_{XC} + v_{ext} \quad (1)$$

Where $-\frac{1}{2}\nabla^2$ and v_H are the kinetic energy and the electron-electron repulsion energy, respectively and v_{XC} is the exchange correlation energy and v_{ext} is the external potential. The $\rho(r)$ of a system can be obtained by summing over the individual single-electron wave functions

$$\rho(r) = \sum_{\mu} |\chi_{\mu}|^2 \quad (2)$$

The single-electron wave functions can be expanded using a plane wave basis (representing the orbital in Fourier space) and solved using the Kohn-Sham equations [5]. In most DFT codes, the ionic potential is removed and replaced by a pseudo-potential term, restricting the wave function and potential to within a core radius. This approach may make the calculation more computationally efficient. However, a large number of plane waves are typically required to converge the properties of interest (over 100 per atom), particularly for the compact $2p$ orbitals of hydrogen atoms. The elegance of the technique lies in the fact that a single determinant describes the electron density - all of the complexity is bundled into the exchange-correlation functional. Unfortunately though, this simplicity is rather a double edged sword. Limitations arising from errors in the standard density-functionals, namely the delocalisation error and fractional charges, and the static electron correlation error and fractional spins have been discussed in the Science paper by Cohen *et al.* [6]. They highlight the following problem: for a calculation on a system involving a single electron, an artificial energy arises from the density of the electron interacting with the electron itself, this is known as a self-interaction error (SIE). This should, in theory be fairly easy to correct for, by evaluating the self-interaction terms and removing them. However, the manifestation in many electron systems is extremely difficult to quantify, and as yet, no method has managed. In a similar way, errors are also produced for the spin-spin interaction.

The Projector Augmented-Wave (PAW) method was invented by Peter Blöchl in 1994 [7] to calculate the electronic properties of materials within a DFT framework. The method is well suited to problems in the solid state and builds upon the advantages gained from pseudo-potential calculations, providing the correct nodal behaviour in valence electron wave functions while providing a description of full all-electron wave functions and density. The main advantage in this context is that since it deals with a full valence electron wave function, an accurate description of the electron spin density at the nucleus is provided. Full details of this type of calculation can be found in Blöchl's review [7]. It was successfully applied to muoniated ethanal by Probert and Fisher where they simulated both zero-temperature and thermally averaged values for the hfcc's [46]. There are a few packages that implement the PAW method, including Quantum ESPRESSO, CASTEP and GPAW.

1.2 Basis sets

The Basis Set is described by a set of functions which are used to describe the molecular orbitals within a system. We can express the MOs of a system as a linear combination of atomic orbitals (LCAO). The main strength of this LCAO approach is that it well suited to molecular systems, containing any number of atoms. It is possible to implement a greater number of AOs in the approach, e.g., to describe hydrogen, we can use more than one s AO, and also include some p and d AOs. A larger number of AOs will provide an increased flexibility of the MO, therefore improving the accuracy of the calculated properties. There are two main types of these basis functions, Slater Type orbitals (STO) [8] and Gaussian Type Orbitals (GTO) [9].

Basis sets differ in the number of component functions used. The *minimal basis set* employs a single Slater function or its Gaussian counterpart for each occupied atomic orbital in the ground state. For example, hydrogen would be described by a single s -function and carbon would be described by two s -functions and a set of 3 p -functions. The most popular *minimal basis set* is the STO- n G, where n is the number of Gaussian functions. The STO-3G is a *single zeta (SZ)* basis set; implementing three primitives per function. The valence orbitals play a greater role in chemical bonding than core orbitals, as such a more sophisticated basis set is required in order to better model valence orbitals. Basis sets can be improved by increasing the number of basis functions per atom. Split valence basis sets do just this, and can be expressed as a - bcd G, where a represents the number of primitives used for inner shells and bcd are the number of primitives used in the valence shell. Doubling, tripling or quadrupling all the basis functions give what are referred to as *double zeta (DZ)*, *triple zeta (TZ)* and *quadruple zeta (QZ)*, respectively. A popular example is the 6-31G basis set; a DZ basis set, in which the core orbitals are described by six primitive GTO and the valence orbitals are represented by two functions, with the first composed of three primitive GTO, while the second consists of a single GTO.

Split valence basis sets can be further improved through the addition of polarisation and diffuse functions. Polarisation functions have higher values of angular momentum than those present on a particular orbital on an atom in the ground state. For example, the p -orbital introduces polarisation to the s -orbital, and the d -orbital adds polarisations to the p -orbital. This polarisation allows the shape orbital to be modified so as to better cover a bonding region between two atoms. The molecular orbital (MO) of anions and excited states have a tendency to be more spatially diffuse than ground state MO's. To account for this, basis sets are augmented with diffuse functions which essentially increase the size of the orbital. An infinite number of basis functions would be required to perfectly

describe an orbital. In reality, the number of functions present within a basis set is limited. An error is therefore inherent in the description of the orbital; this is known as the Basis Set Limit.

Increasing the complexity of the system, i.e. increasing the number of electrons present, increases the computational expense. Heavier elements such as transition metals and elements from the lower end of the Periodic Table have large numbers of core electrons, and thus require a large number of basis functions to describe them. In a chemical sense, these electrons are fairly unimportant, since it's the valence electrons that are involved in chemical bonding. However, if these core electrons were excluded from the calculation, the valence electrons would be inadequately described - due to a poor description of electron–electron repulsion. So, in chemical systems that contain heavy elements the user can describe them in one of two ways: by treating all the electrons implicitly, resulting in huge computational expense (the calculation will take forever to finish - most high performance computer facilities impose a run time, typically five to seven days; the job automatically terminates after this time has been exceeded); or alternatively, the valence electrons can be treated explicitly and the core electrons may be replaced by an analytical function known as an Effective Core Potential (ECP) [10,11]. From a computational perspective this is a much more efficient approach, and is common practice in modelling systems involving heavier elements. For calculating magnetic properties however, the literature advises using small ECP [12].

Calculating magnetic properties requires a basis set with a high level of flexibility in the core region, and basis sets such as the EPR-II and EPR-III offer this flexibility, particularly in conjunction with the B3LYP functional [41]. EPR-II is a double zeta basis set has a single set of polarisation functions, with an enhanced *s* function, while the triple-zeta EPR-III basis set includes diffuse functions, double *d*-polarisations and a single set of *f*-polarisations.

1.3 Practical considerations

There are numerous software packages that facilitate calculation of hfcc's. Packages such as Gaussian [13] and Vienna Ab initio Simulation Package (VASP) [14] require licences, restricting their accessibility. There are also open source packages available, examples include Quantum ESPRESSO [15], GAMESS [16], Amsterdam Density Functional (ADF) [17], ORCA [18], GPAW [19], and CASTEP [20], all are very well maintained. However, whichever package is chosen, access to a high performance computer facility (such as the SCARF facility [21], open to all STFC departments and Diamond) is essential. Recent advances have seen electronic structure algorithms being reformulated for Graphical Processing Units (GPU), making DFT calculations on large systems (10^3 atoms) feasible. In any case, overcoming a steep learning curve is required to compile the input file for the calculation, and specialist 'first principles' knowledge required to extract meaningful results.

The input of a typical DFT calculation (see Appendix) requires specification of the number and types of atoms present in the molecule, their atomic coordinates, the charge, and multiplicity of the molecule, and definition of model chemistry (theoretical method and basis set). Armed with these parameters, the structure of a molecule and its properties, such as hfcc can be calculated. In order to predict the magnitude of the hfcc, it is crucial to have an accurate description of the spin density at nuclear positions (requiring an accurate optimised structure!). This is reliant on a suitable choice of basis set, and given that each has a limited atomic palette (see [The Basis Set Exchange - https://bse.pnl.gov/bse/portal](https://bse.pnl.gov/bse/portal)) and suitability for particular applications, this will be the first of many

difficulties that a novice user would encounter. Typically, it would be advisable to consult the literature to ensure the suitability of a choice, as some methods are clearly more adept at simulating hyperfine parameters than others; however, given that most systems that would be used in the linked software would likely be small and organic in nature; there is scope to provide guidance on choice of model chemistry used within the software. Since most software packages (with the exception of ADF) do not allow the muon to be modelled explicitly within the initial geometry optimisation calculation, a proton is frequently used in the muons' place. Clearly, the difference in mass between the muon and the proton must be accounted for, as must the effects of any dynamics or solvation present. These factors add complexity to the calculation, and mean a complicated model must be used to account for them [22]. Again, to help the user, it may be possible to include such models as part of an integrated software package, provided one has the time and computer power.

So far, we have dealt with the input of a typical calculation, but one question which quickly arises when starting out in this field is how to get the structure in the first place. Input structures can be obtained from crystal structure databases such as the Cambridge Structural Database (CSD). Alternatively, they can be drawn from scratch using appropriate visualisation software. Again, there are a plethora of software packages available; Gaussview, CAChe (Scigrass Explorer), HyperChem, MOLEKEL, Chem3D, and gOpenMol all offer compatibility with Gaussian. No one package is *better* than another, the choice comes down to personal preference, and more importantly, if it's free.

1.4 μ SR theoretical background

In this paper we are particularly concerned about the use of DFT methods to calculate muon-electron and nuclear-electron hfcc's to assist the interpretation of Avoided Level Crossing (ALC) μ SR experiments.

During thermalisation, a large proportion of muons that are implanted into organic species capture an electron to form muonium, Mu or μ^+e^- . The spins of the muon and the electron interact through the hfcc. Muonium can rapidly react with centres of unsaturation (double or triple bonds) to form a paramagnetic species known as a muoniated radical [23, 24]. The classic addition involves the formation of a simple covalent bond, with one electron being supplied from muonium, and one electron being supplied from the C=C bond (Figure 1). Pictorially, this leaves an unpaired electron on the beta-carbon atom, but in reality the unpaired electron is often distributed throughout the molecule.

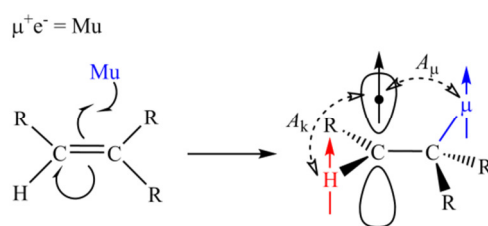


Figure 1. Schematic showing muonium addition, producing a muoniated radical.

Depending on the circumstance, the hfcc can have isotropic and anisotropic components. Vacuum muonium can be described by a 1s hydrogenic like wavefunction in which the electron spin, \vec{S}_e , and the muon spin, \vec{S}_μ , is described entirely by the isotropic hfcc, A . Blundell's review [25] demonstrates that inclusion of the Zeeman terms into the Hamiltonian gives:

$$H_0 = -\gamma_\mu \vec{S}_\mu \cdot \vec{B} + \gamma_e \vec{S}_e \cdot \vec{B} + A \vec{S}_\mu \cdot \vec{S}_e \quad (3)$$

and that if this two-spin system is defined by Pauli spin matrices, four energy eigenvalues follow [25]:

$$E_{|\uparrow_\mu \downarrow_e\rangle} = E_1 = \frac{\hbar}{4} [A + 2B(\gamma_e - \gamma_\mu)] \quad (4)$$

$$E_{|\uparrow_\mu \downarrow_e\rangle + |\downarrow_\mu \uparrow_e\rangle} = E_2 = -\frac{\hbar}{4} \left[A - 2\sqrt{A^2 + B^2(\gamma_e + \gamma_\mu)^2} \right] \quad (5)$$

$$E_{|\downarrow_\mu \downarrow_e\rangle} = E_3 = -\frac{\hbar}{4} [A - 2B(\gamma_e - \gamma_\mu)] \quad (6)$$

$$E_{|\uparrow_\mu \downarrow_e\rangle - |\downarrow_\mu \uparrow_e\rangle} = E_4 = -\frac{\hbar}{4} \left[A + 2\sqrt{A^2 + B^2(\gamma_e + \gamma_\mu)^2} \right] \quad (7)$$

The Breit-Rabi diagram in Figure 2 shows that in the absence of a magnetic field the system has two energy levels, a lower energy singly degenerate $\frac{1}{4}A$ state and a higher energy triply degenerate $-\frac{3}{4}A$ state, these are separated by an energy equal to the hfcc. The degeneracy of the triplet state is lifted when a magnetic field is applied, and we now have a system with four distinct energy levels (see Figure 2). At high magnetic fields, these energy levels can begin to converge on one another, becoming nearly degenerate. In the case of vacuum muonium levels 1 and 2 converge at about 16.4 Tesla ($A=4.46$ GHz).

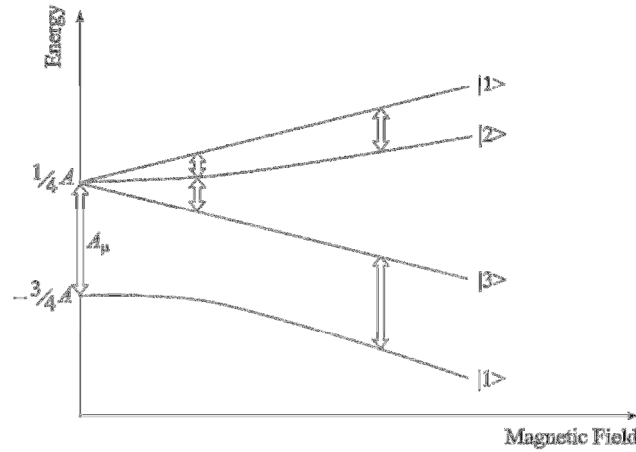


Figure 2. Breit-Rabi diagram for isotropic muonium.

The anisotropic component of the hfcc is due to the magnetic dipole interaction between the unpaired electron and the nucleus. The full Hamiltonian ($H_{full}=H_0+H_{\mu,aniso}+H_{nuclei}$) for a three spin system including axial asymmetry, and perpendicular dipolar parameters, D_i ($i=\mu,k$) (describe the anisotropy of the system) has been described in detail by Roduner [26] and more recently in a review by Nuccio *et al.* [27].

1.4.1 Transverse field- μ SR

Application of a transverse magnetic field (TF) is one method that is used to gain access to the muon hfcc. In low magnetic fields, the muon polarisation can be distributed between all spin states, making the hfcc inaccessible. In higher magnetic fields, or in the region more commonly known as the Paschen-Back regime, the Zeeman energy begins to dominate, and only differences between levels E_1 and E_2 , and between E_3 and E_4 can be observed (see Figure 2). These precession frequencies are described by [28]:

$$f_{12} = \frac{1}{2}A + \frac{1}{2}(\gamma_e - \gamma_\mu)B - \frac{1}{2}A \sqrt{1 + \left(\frac{2B(\gamma_e + \gamma_\mu)}{A}\right)^2} \quad (8)$$

$$f_{34} = \frac{1}{2}A + \frac{1}{2}(\gamma_e - \gamma_\mu)B + \frac{1}{2}A \sqrt{1 + \left(\frac{2B(\gamma_e + \gamma_\mu)}{A}\right)^2} \quad (9)$$

Following Fourier transformation, the frequency spectrum of such a system is characterised by a strong diamagnetic peak, resulting from μ^+ precessing at its Larmor frequency, and a pair of resonances placed symmetrically about this diamagnetic signal. It is the sum of these two frequencies that defines the muon hfcc. Since the wave function of the unpaired electron in a muoniated radical is often spread over the molecule, the magnitude of the hfcc is always characteristic of the muon binding site. In a TF- μ SR experiment, a pair of precession frequencies corresponding to each binding site is present. Figure 3 shows such a spectrum for the muoniated cyclohexadienyl radical, with a pair of signals at 208.52 MHz and 305.48 MHz corresponding to a muon hfcc of 513.86 MHz, at 305 K (Figure 3, right). Curiously, the feature it split, and this probably merits further investigation.

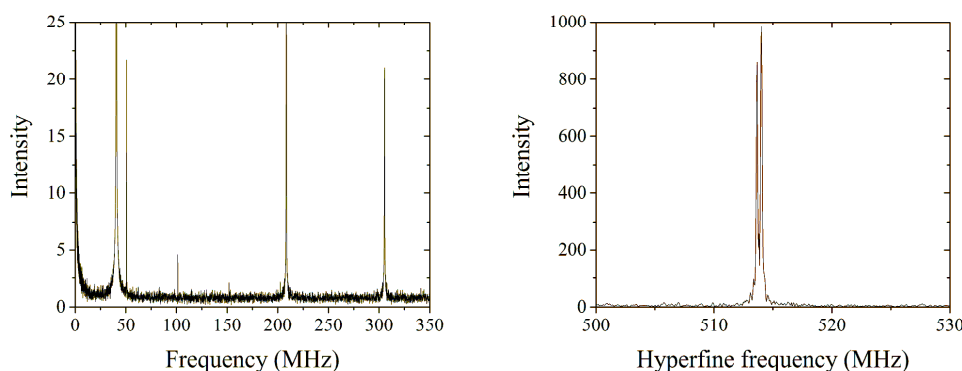


Figure 3. (Left) TF- μ SR spectrum from muoniated benzene at 305 K in a magnetic field of 3 kG. The spectral feature at 40.67 MHz (truncated) is from muons in the diamagnetic environment, the pair of signals at 208.52 MHz and 305.48 MHz are from the muoniated cyclohexadienyl radical. (Right) Correlated spectrum indicating a hfcc of 513.86 MHz for the muoniated cyclohexadienyl radical at 305 K (unpublished data).

1.4.2 Avoided level crossing- μ SR

The technique of Avoided Level Crossing (ALC)- μ SR is capable of revealing both muon and nuclear hfcc's, but it is often easier to initially perform a TF- μ SR experiment to identify the muon hfcc,

before using ALC to identify any nuclear couplings. The technique involves consideration of anisotropic contributions to the hfcc, and also additional spin-active nuclei. Anisotropy is usually present in muoniated radicals in the solid phase, and averages to zero in liquid and gaseous phases where the reorientation rate of the molecule becomes larger than the dipolar interaction. The spin of the muon, the unpaired electron, and any other spin active nuclei form a quantised system characterised by a series of discrete energy levels. At characteristic magnetic fields determined by the chemical system, two energy levels in the system can become nearly energy degenerate and are able to interact through the isotropic and anisotropic components of the hfcc. During this interaction the muon spins may oscillate between the two energy states, and thus, as the resonance is scanned, a reduction in the muon polarisation is observed (see Figure 3). The magnitude of the muon-electron, A_μ and nuclear-electron, A_k are characteristic of the muon binding site, and give rise to ALC resonances whose position are dependent upon their magnitude. The selection rule $|\Delta M|=0, 1$ and 2 (Δ_0 , Δ_1 and Δ_2 resonances, respectively) determine the type of resonance, where M represents the sum of z components of the muon, electron, and nuclear spins.

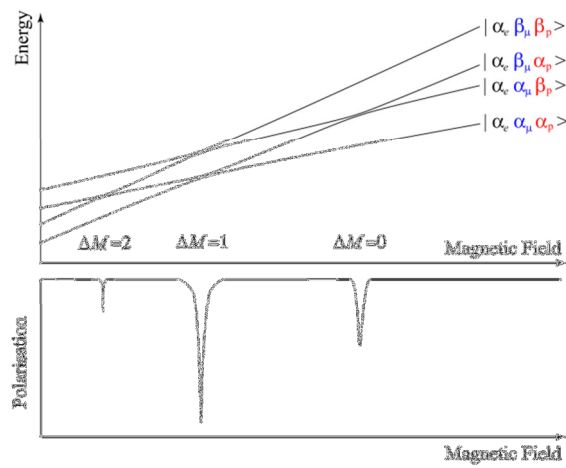


Figure 3. Breit-Rabi diagram at high magnetic field showing the energy levels of a three spin system, indicating the three types of avoided level crossing.

The field at which Δ_0 resonances appear is given by:

$$B_{res}^{\Delta_0} = \frac{1}{2} \left(\frac{A_\mu - A_k}{\gamma_\mu - \gamma_k} - \frac{A_\mu + A_k}{\gamma_e} \right) \quad (10)$$

γ_μ , γ_k and γ_e represent the gyromagnetic ratios of the muon, proton and electron, respectively.

The Δ_1 resonance field position can be predicted by:

$$B_{res}^{\Delta_1} = \frac{1}{2} \left(\frac{A_{e\mu}}{\gamma_\mu} - \frac{A_{e\mu}}{\gamma_e} \right) \quad (11)$$

The position of the the ALC resonance is dictated by the magnitudes of the isotropic hfcc's, while the dipolar parameters are responsible for the lineshape and width [24, 26, 27].

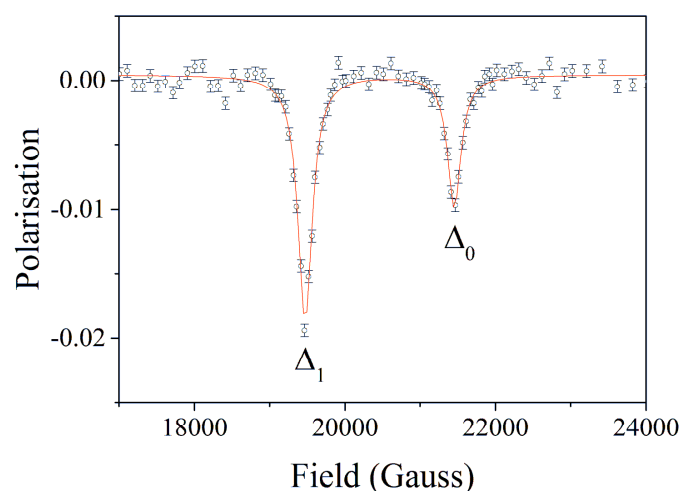


Figure 4. ALC- μ SR spectrum of the muoniated cyclohexadienyl radical at 210 K (unpublished data).

Figure 4 shows the Δ_1 (1.9471 Tesla) and Δ_0 (2.1453 Tesla) resonances of the cyclohexadienyl radical at 210 K. Calculating the muon and nuclear hfcc therefore enables an estimation of the resonance positions, prior knowledge of which has the potential to save valuable beamtime by allowing the experimenter to scan only the necessary field regions. The experimenter is also able to assign resonances to nuclei and identify the muon binding site through comparison of the measured and simulated hfcc. However, an understanding of the accuracy to which these values can be calculated is required to avoid discrepancies in assignment. The choice of theoretical method and basis set goes a long way to “reliably” predicting the magnitude of the hfcc, and is strongly affected by the model used in the optimisation to obtain the structure, and in the model chosen for the calculation of hfcc’s (they need not be the same model). Some may appear to work well for predicting the properties of basic organic radicals, but this is often due to a fortuitous cancellation of errors. The upshot of this is that when the same method applied to radicals containing many electron atoms, the simulation gives values which are far from realistic.

The choice of model chemistry is often derived through validation against a training set of molecules, and using the results to produce a scale factor. Much work has been done in the areas of simulating Nuclear Magnetic Resonance (NMR) [29] and Electron Paramagnetic Resonance (EPR) [30, 31, 32] using DFT; these studies prove useful in providing information on suitable model chemistries. However, for calculating the hfcc’s of muoniated radicals, a reliable method of accounting for the isotope effect is required to bring results from even the best model chemistry close to those of experiment. Hudson and Chafetz demonstrate this for the cyclohexadienyl muoniated radical [33].

2 Developing a model for the muoniated cyclohexadienyl radical

2.1 Evaluating popular DFT methods

The review from Improta and Barone [22] discusses the validity of various quantum mechanical models for calculating hfcc’s. Their survey compared simulated spin densities of the methyl radical using empirical, semi-empirical, and non-empirical quantum mechanical calculations. The results

clearly demonstrate the need to include electron correlation in order to provide semi-quantitative agreement with experimental observations. The effectiveness of semi-empirical, Hartree-Fock, and DFT methods have also been evaluated in the work of Batra *et al.* [32], where a selection of small organic molecules were selected as prototype systems. However, the cyclohexadienyl muoniated radical was one of the first to be studied using the μ SR technique [34], and is now considered a classic prototype system in muoniated radical chemistry [24, 35]. We therefore use this system to evaluate the effectiveness of various theoretical models, starting simple and building in complexity.

When muonium reacts with an unsaturated C=C bond in benzene, the muoniated cyclohexadienyl radical is formed, with the unpaired electron density delocalised throughout the ring (Figure 5). It is therefore possible to observe the muon-electron, A_μ hyperfine coupling, as well as the *ipso* nuclear-electron coupling. *Ortho*, *meta* and *para* couplings are possible in theory, but their distance from the muon makes them difficult to observe. Yu *et al.* reported TF and ALC μ SR measurements of the cyclohexadienyl muoniated radical at 293 K, with hfcc's of $A_\mu = 514.807$ MHz for the muon and $A_k = 126.133$ MHz for the *ipso* proton [36]. Here, we compare this data (calculated from least squares fitting) with values from static gas phase calculations at 300 K obtained using a selection of popular functionals (HF, TPSS [37], B3LYP [38], PBE [39] and PBE0 [40]) all in combination with the EPR-III [41] basis set (Table 1). All of the calculations use a proton in place of the muon, and we account for the larger gyromagnetic ratio of the muon relative to the proton, by scaling A_μ values by a factor of 3.183. However, since the structure was geometry optimised as a protonated radical, the C- μ and the C-H (*ipso*) bond lengths are unrepresentative of a muoniated radical. Consequently, the magnitudes of A_μ and A_k (*ipso*) appear to be significantly underestimated. The most computational inexpensive model, HF/EPR-III provides the best overall agreement; underestimating A_μ by 18.5 MHz (3.6 % error), and overestimating A_k by 29.8 MHz (23.6 % error) compared to the experimental values. Practically, in the setting of an ALC type experiment, this corresponds to a 686 Gauss and 2601 Gauss difference in the magnetic field positions of the Δ_1 and Δ_0 resonances, respectively. This magnitude of error is too large for the calculations to be considered useful, especially when considering application to more complicated systems where numerous radical species are possible, and the aim of the calculation is facilitate identification of the radical structure.

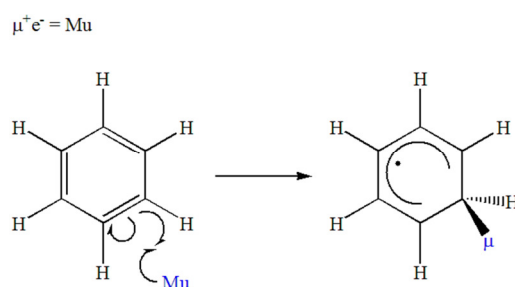


Figure 5. muonium addition to benzene.

	A_μ (MHz)	$\Delta_1 B_{res}$ (Gauss)	A_k <i>ipso</i> (MHz)	$\Delta_0 B_{res}$ (Gauss)
Exp. ^(a)	514.8	19088	126.1	20798
HF	496.3	18402 (686)	155.9	18197 (2601)
TPSS	477.1	17692 (1396)	149.9	17495 (3303)
B3LYP	479.7	17785 (1303)	150.7	17587 (3211)
PBE	485.5	18001 (1087)	152.5	17801 (2997)
PBE0	473.7	17563 (1525)	148.8	17368 (3430)

mp2	370.7	13746 (5342)	116.5	13593 (7205)
------------	-------	--------------	-------	--------------

^(a) Calculated from a least-squares fit of data in reference [36].

Table 1: Comparison of experimentally determined and simulated A_μ and ipso A_k hyperfine coupling constants of the cyclohexadienyl muoniated radical at 293 K. Values in parentheses represent the difference from the experimental value. Calculations use a selection of functionals with the EPR-III basis set, for geometry optimisation and the single point energy calculation that generated the hfcc.

Table 2 is purely illustrative; to show how changing the description of the orbitals with different basis sets can affect the magnitude of the A_μ .

	A_μ (MHz)	$\Delta_1 B_{res}$ (Gauss)	A_k <i>ipso</i> (MHz)	$\Delta_0 B_{res}$ (Gauss)
Exp. ^(a)	514.8	19088	126.1	20798
STO-3G	364.8	13527 (5561)	114.6	13376 (7422)
3-21 G	391.0	14497 (4591)	122.8	14336 (6462)
6-31 G	473.4	17552 (1536)	148.7	17356 (3442)
6-31 G**	449.0	16648 (2440)	140.8	16476 (4322)
6-311 G**	439.4	16293 (2795)	138.0	16111 (4687)
EPR-II	462.8	17161 (1927)	145.4	16970 (3828)
EPR-III	479.7	17785 (1303)	150.7	17587 (3211)

^(a) Calculated from a least-squares fit of data in reference [36].

Table 2: Comparison of experimentally determined and simulated A_μ and *ipso* A_k hyperfine coupling constants of the cyclohexadienyl muoniated radical at 293 K. Values in parentheses represent the difference from the experimental value. Calculations use the unrestricted B3LYP functional in combination with a selection of basis sets, for geometry optimisation and the single point energy calculation that generated the hfcc.

2.2 Considering the isotope effect

The hfcc is extremely sensitive to the isotope effect. Compared to a hydrogenated radical, the magnitude of A_μ in a muoniated radical has been reported to be as much as 30–40 % greater (at 300 K) [42]. An unfortunate caveat of the DFT methodology is that nuclei are treated as point charges, and the nuclear quantum effect is not included. In many calculations previously reported for muoniated radical systems, a scale factor is used to lengthen the muon bond post optimisation, and a single point energy calculation is then used to calculate magnetic properties [36, 43, 44]. Lopes de Magalhães and Ramos used a Morse potential to calculate the average interatomic distances of C–H and C– μ (1.141 Å and 1.197 Å, respectively) [45]. To identify any additional isotope induced perturbations they increased the C– μ bond length by 4.9 %, fixing it at this length while they re-optimised the structure. Interestingly, they found that the *ipso* C–H bond length in the resulting structure was 0.3 % shorter. In order to test the validity of this simple method, the cyclohexadienyl hydrogenated radical was re-optimised, with a C–H bond (corresponding to the C– μ) lengthened by 4.9 % and fixed during the subsequent minimisation using the uB3LYP/EPR-III model chemistry. As before, the resulting A_μ value was scaled by 3.183. The method overestimates A_μ by 10.3 MHz (2 % error) at 300 K, which in the ALC spectrum would correspond to an overestimation of the Δ_1 resonance position by 196 Gauss. In an ALC experiment running at 300 K, the Δ_1 resonance can be characterised by scanning from 1.84 Tesla to 2.2 Tesla with a 20 Gauss step size. If however, this was an unknown system, and we only have the calculated hfcc, the resonance could be found by scanning the region coarsely in a relatively small amount of time. For example, with 50 Gauss steps, counting 4 MeV/point and assuming a count rate of 90 MeV/hr, it would take approximately 40 minutes to scan the area between 1.89 Tesla to 1.96 Tesla to identify the resonance. The region could then be probed in more detail to fully characterise the resonance lineshape. On the face of it, a 2 % error would be acceptable to use the method to aid experiment.

	A_μ (MHz)	$\Delta_1 B_{res}$ (Gauss)	A_k <i>ipso</i> (MHz)	$\Delta_0 B_{res}$ (Gauss)
Exp. ^(a)	514.8	19088	126.1	20798
B3LYP/EPR-III	525.1	19284 (196)	141.6	20514 (284)

^(a) Calculated from a least-squares fit of data in reference [36].

Table 3: Comparison of experimentally determined and simulated A_μ and *ipso* A_k of the cyclohexadienyl muoniated radical at 293 K. Calculations employ a selection of functionals in combination with the EPR-III basis set. Following the geometry optimisation, the C- μ bond distance was increased by 4.9 % and the structure re-optimised, to account for the isotope effect [43].

The model predicts the magnitude of A_μ at 300 K with a 2 % error, but is only useful to us if it can predict A_k couplings with a similar level of accuracy. We found that the *ipso* A_k coupling was similarly overestimated, by 15.5 MHz using the B3LYP/EPR-III level of theory. However, the errors of A_μ and A_k propagate through equation 10, meaning that the Δ_0 resonance is predicted to be 284 Gauss lower than the experimental resonance position. Just as discussed for the Δ_1 resonance, despite this error these DFT results provide a valuable tool for the resonance search; however, the error is likely to make an unambiguous assignment of a spectrum measured for a more complex molecular system difficult. Couplings for the *ortho*, *meta*, and *para* protons can be easily calculated in our muoniated cyclohexadienyl radical system, but experimental data associated with these is more difficult to come by. It would be interesting to see if these were systematically overestimated by this method; in which case a simple scale factor could be added to each. It is very likely however, that the method produced these values in a fortuitous cancellation of errors, and the method is unlikely hold true in more complicated systems. For systems where multiple muonium addition sites exist, the task of structural assignment becomes problematic, and the locations of Δ_1 resonances (A_k couplings) become integral to the task. However, the more addition sites, the weaker the intensity of Δ_0 and Δ_1 resonances from each radical, and in polar systems the systematic overestimation of A_k couplings would no longer hold.

2.3 Vibrational averaging

In order to reliably predict the magnitude of both A_μ and A_k couplings, it is therefore necessary to apply zero-point vibrational corrections for comparing with high temperature data. However, validating the method relies on having hfcc temperature dependence data down to low temperatures, as close to 0 K as possible. Previous attempts at calculating the temperature dependence of the hfcc using a Boltzmann average of vibrational and rotational modes proved relatively unsuccessful [46].

Before proposing a methodology for ZPE vibrational averaging, a little more background information if required. The structure of a hypothetical molecule, ABC can be described by the geometric locations of nuclei A, B and C. For any given structure or electronic state, ABC has a specific energy. The Born-Oppenheimer approximation allows the motions of the nuclei and electrons to be separated – the nuclei are much heavier than the electrons, so they move much more slowly. However, it is when dealing with small nuclei, such as the muon, that the approximation begins to fail. In any case, the Born-Oppenheimer energy of a molecule is obtained by determining the electronic wave function for a set of fixed nuclear positions. The Potential Energy Surface (PES) describes the relationship between the locations of A, B and C and the energy. During a geometry optimisation, atoms A, B, and C are arranged so as to minimise the energy, giving the equilibrium geometry. The nuclei of the molecule are not static, but rather vibrating about their equilibrium positions. A molecule composed

of n atoms will have $3n-6$ fundamental modes of vibration (or $3n-5$ for linear molecules). If we plot the total energy of ABC as a function of one of the displacements described by a normal mode, the A–B stretch for example, we get a one dimensional Morse like PES. ABC does not reside at the bottom of this curve, but instead occupies one of the vibrational energy levels. If we have a group of ABC molecules, the energy levels are populated according to the temperature and the inter-level spacing ($E_n = (n + \frac{1}{2})h\nu_0$). When discussing isotope effects, we are only really concerned with the vibrational contributions – namely the zero-point and temperature dependant vibrational contributions. The ZPE is the difference in energy between the vibrational ground state and the lowest energy point on the Born-Oppenheimer PES, the energy of which is equal to $(n + \frac{1}{2})h\nu_0$. Vibrational effects have been largely ignored when calculating hfcc for larger radical species [47, 48], and also for smaller organic radical species in some cases [49].

For our prototype system, the muoniated cyclohexadienyl radical, this so called local mode approach applies a vibrational correction to the C–H(μ) degrees of freedom. Similar approaches have previously been demonstrated for a series of cycloalkanes in a paper by Yang and Hudson [29] and more recently by Hudson and Chafetz in their study of the isotropic perturbations induced in the cyclohexadienyl muoniated radical [33]. In the latter example, the authors calculated the average isotropic hfcc across the C– μ stretching, as well as the in plane and out of plane bending motions. Here, we apply and test a similar methodology to the muoniated cyclohexadienyl radical using a combination of a variety of functionals and basis-sets. The results of these ZPE vibrational corrections can be compared to the low temperature experimental data collected by Fleming *et al.* [35] (see Figure 6). Notably, the authors did not record a full data set extending back to T=0. Instead, we have a limited experimental dataset from 313 K to 170 K. Using the liquid state data and extrapolating back to T=0 gives a hfcc of 537.2 (± 1.2) MHz, but this is a non-ideal representation of benzene at T=0. Benzene has a freezing point of 278.65 K, meaning only six of the data points are in the solid state (Figure 6). Extrapolating the solid state data gives an $A_0=553.0$ (± 1.6) MHz. However, this is not without its problems either; here we assume A_μ continues to have linear temperature dependence down to T=0 K. Fleming’s data indicates a splitting of the $\Delta M=1$ resonance below ~ 180 K, suggesting the possibility of multiple cyclohexadienyl radical environments, and possibly a non-linear A_μ temperature dependence [35]. Preliminary low temperature data on the muoniated cyclohexadienyl radical from a recent ISIS experiment [50] confirm this splitting, and the full analysis should reveal the nature of the A_μ temperature dependence. Fleming *et al.* also included limited temperature dependant hfcc data for H_{ipso} , with three data points reported in the solid state [35] (Figure 6). This A_k data ($\times 3.183$) is extrapolated to T=0 (426.4 MHz), and used with the extrapolated solid state A_μ data to give an experimental quantum factor, 1.297 which we can use for internal calibration.

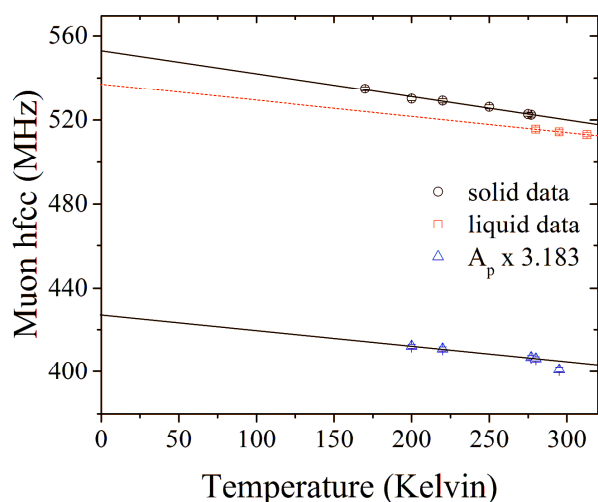


Figure 6. A_μ temperature dependence for the $[C_6H_6\mu]^\bullet$ radical, using data compiled from [35].

2.3.1 C- μ stretching vibration

The cyclohexadienyl radical was first geometry optimised, imposing C_{2v} symmetry. The optimised structure was taken as input for two further calculations. The first of which was a single-point energy calculation where the muonium isotope was specified (in Gaussian this is done by invoking the *freq=(readisotopes)* keyword), this generated the $3N-6$ normal modes of vibration for the muoniated cyclohexadienyl radical that will be used later in the averaging process. The second calculation involved displacing one of the equivalent C–H bonds along its stretching path (corresponding to a mode at 2096 cm^{-1} in $[C_6H_7]^\bullet$ and 8398 cm^{-1} in $[MuC_6H_6]^\bullet$), from 0.6 \AA to 3.6 \AA in 0.1 \AA increments. This may be done manually. In this case, the optimised structure is opened in a molecular viewing package, and modified structures associated with each incremental bond change are saved as input files for subsequent energy and hfcc calculations. It is possible to input all these structures into a single input file (using the Gaussian `–Link1–` command) and have Gaussian calculate the properties associated with each structure in an iterative manor, writing the results in a single output file. The advantage of this method is that both the energy and the hfcc can be computed together. The resulting energy (reported in Hartrees) can be easily extracted from the output file to a new parameter file (using the command-line utility *grep*). Alternatively, for a more automated approach, Gaussian offers an option to scan the energy of a parameter such as bond length or bond angle in what is known as a rigid PES scan. In order to do this however, the molecular structure must be specified as a Z-matrix¹. For a rigid PES scan calculation, Gaussian requires an initial value of the parameter, the number of steps, and the step size. Results for each increment can be easily extracted from the output file using, for example, Gaussian Output Tools ([GOT - http://gaussot.sourceforge.net/](http://gaussot.sourceforge.net/)). The energy values can be converted into a more convenient unit of energy such as cm^{-1} , plotted against the corresponding stretch displacement, and fitted by a Morse potential [51]:

$$U_M(r) = D_e(1 - e^{-\alpha(R-R_e)})^2 \quad (12)$$

¹ The atoms in a molecule are listed in such a way so the position of the first atom is treated as the origin, the position of the second atom is defined by a distance from the first. The position of the third atom is defined by its distance from either the first or the second and the angle made from the three atoms. The position of the fourth atom is defined by a bond distance, a bond angle and a torsional bond angle from the previous three atoms. The parameters are listed at the end of the file

Figure 7 (left) shows the Morse potential fit to a C–H displacement, and offers a good fit around the base of the PES ($\chi^2=0.9946$). The Wei four-parameter potential [52](Figure 7 (right)) however, provides a better fit around the PES minima ($\chi^2=0.9983$).

$$U_M(r) = D_e \left(\frac{1 - e^{-a(c-1)(R-R_e)}}{1 - ce^{-a(c-1)(R-R_e)}} \right)^2, |c| < 1 \quad (13)$$

However, we are only interested in the area around the PES minima, and while a polynomial provides an inadequate fit of energy across the entire displacement, it does give an excellent fit across the area of interest, the PES minima ($\chi^2=0.9999$), see figure 8.

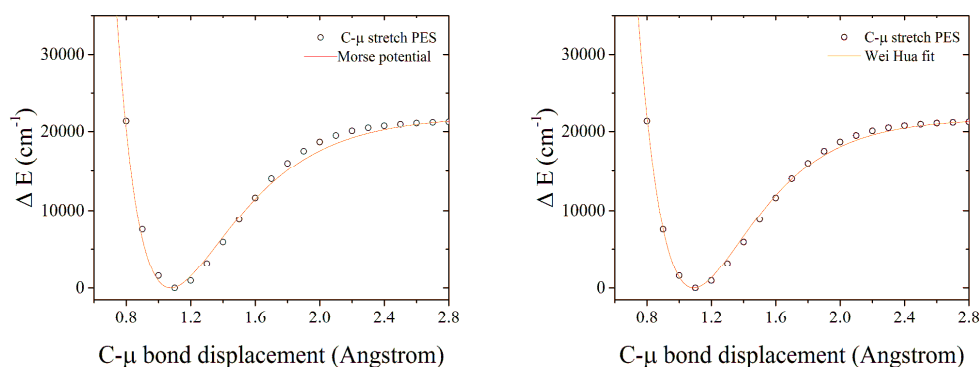


Figure 7. (Left) Morse potential fit to the C–H bond displacement simulated for the C_6H_7 radical using a B3LYP/EPR-III model chemistry. (Right) Wei Hua four parameter fit to the C–H bond displacement simulated for the C_6H_7 radical using the uB3LYP/EPR-III model chemistry.

Although we are clearly dealing with an anharmonic potential, the harmonic approximation does provide an adequate description of the PES for low vibrational energy levels. The ZPE can therefore be found from $\frac{h\nu_0}{2}$, for the C– μ stretching vibration at the B3LYP/EPR-III level of theory, this corresponds to 4199.24 cm^{-1} (illustrated by a blue line in Figure 8). At low and ambient temperatures, only the $v=0$ level is populated, although if dealing with higher temperatures, a Boltzmann distribution could be used to average the populated energy levels. C–H vibrates approximately harmonically (around the minimum of the PES) about the equilibrium bond distance of 1.10293 \AA (at the B3LYP/EPR-III level of theory). The ground state wave function in a harmonic oscillator can be modelled as a Gaussian distribution centred about the equilibrium bond position, the one plotted in Figure 8 has been normalised for the purpose of illustration.

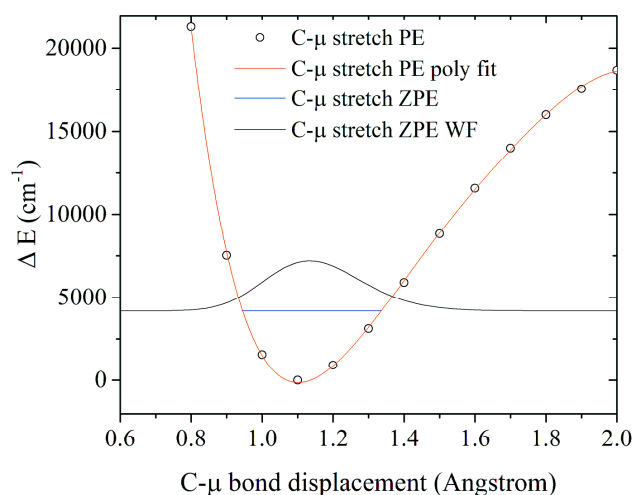


Figure 8. 5th order polynomial fit (red line) to the C- μ bond displacement simulated for the C_6H_7 radical using the B3LYP/EPR-III model chemistry. Blue line indicates the ZPE level for the C- μ stretching vibration, black line indicates the simulated ZPE wave function, normalised to the plot.

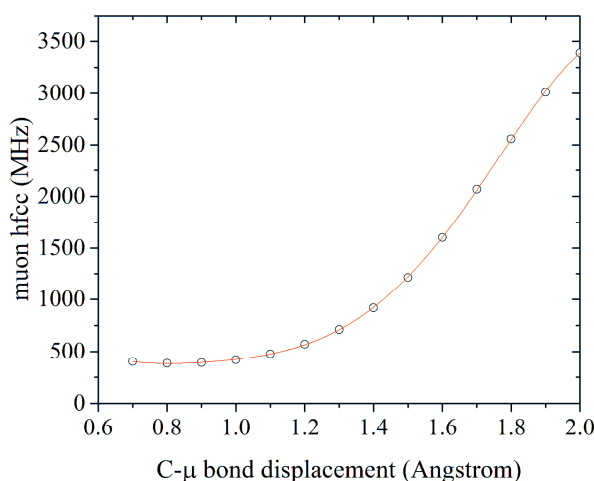


Figure 9. Muon hfcc as a function of C-H bond displacement simulated for the C_6H_7 radical using the B3LYP/EPR-III model chemistry.

The hfcc's were plotted against the displacement values and the results plotted and fitted with an appropriate function (data from the uB3LYP/EPR-III calculations shown in Figure 9 was fitted with a five parameter logistic regression). The hfcc function was then evaluated at the same values of displacement as the normalised square of the wave function, and products of the two determined. The ratio of these products, versus the equilibrium hfcc were calculated, and summed over all the evaluated values to obtain the value P :

$$P = \sum_{i=1}^N \frac{A_i \varphi_i^2}{A_0 \varphi_0^2} \quad (14)$$

The ratio P , and the value produced by summing the normalised square of the wave function were taken to produce the quantum factor, QF :

$$QF = \frac{P}{\sum_{i=1}^N \varphi_i^2} \quad (15)$$

The quantum factor was multiplied by the value corresponding to the equilibrium hfcc, A_0 to give the vibrational zero-point corrected hfcc for the stretching mode of vibration:

$$A_{ZPE} = QFA_0 \quad (16)$$

The procedure was repeated at several levels of theory each using a structure that was geometry optimised at the B3LYP/EPR-III level of theory (Table 4).

	$A_{\mu 0}$ (MHz)	Quantum Factor	A_{μ} ZPE corrected (MHz)
B3LYP/6-31G	469.55	1.225	575.32
B3LYP/6-311++G**	442.64	1.222	540.73
B3LYP/cc-pVQZ	456.12	1.224	558.34
B3LYP/EPR-II	471.50	1.234	581.60
B3LYP/EPR-III	476.35	1.209	576.00
PBEO/EPR-III	461.67	1.214	560.77
PBEO/cc-pVQZ	442.79	1.212	536.84

Table 4: Comparison of zero-point vibrationally corrected muon hfcc's for the C- μ stretch, using a combination of functionals and basis sets. In each case the structure was initially optimised at the B3LYP/EPR-III level of theory.

Due to the method used to simulate the PES for the stretching vibration in this work, the equilibrium bond distance, $R_0=1.10301 \text{ \AA}$ (calculated at the optimised level of theory, B3LYP/EPR-III), is not directly sampled in either the energy or hfcc calculations. Therefore, the values used for $A_{\mu 0}$ in Table 4 are obtained from the fits of hfcc's at each level of theory. $A_{\mu 0}$ calculated at the B3LYP/EPR-III level of theory when calculated during the geometry optimisation has a value of 479.7 MHz (see Table 2). We have therefore unwittingly introduced a 0.69 % error before starting the averaging procedure.

2.3.2 C- μ bending vibrations

The muon is also involved in in-plane and out-of-plane bending motions (torsional motions may well need to be taken into account for less rigid molecules). Vibrations involving the muon in a muoniated radical are, to a large extent, vibrationally isolated - motions involve only the muon. Closer inspection of these vibrations from the simulations shows that for the muoniated cyclohexadienyl radical they are not bending motions in a classical sense (forming an arch with fixed C- μ bond length), but rather translations of the muon in and out of plane of the molecule, which gives a varying bond length (see Figure 10). As such, simulation of their energy was achieved by introducing a ghost or dummy atom, and specifying the change in position (bond length) of the muon with reference to this. Notably, it would be possible to automate the process of calculating energy and hfcc in the same way as used for the stretching vibration. Figures 11 and 12 show the simulated energies and muon hfcc's for the *in* and *out* of plane bending motions using the B3LYP/EPR-III level of theory. Notably, the PES

describing these vibrational modes are harmonic, so a symmetric wave function is easily justifiable. The hfcc's sampled across the so called bending coordinate display a much smaller variation compared to the stretching vibration, with a mean of around 500 MHz for both modes. Table 5 and 6 show the couplings and the vibrationally corrected couplings at the selected levels of theory. $A_{\mu 0}$ values for each of the modes were obtained by evaluating the hfcc fitting functions at the equilibrium bond distance, at each level of theory. Unfortunately, this systematic error is magnified when accounting for the difference in the gyromagnetic ratio, resulting in ~ 3 MHz difference in $A_{\mu 0}$ at the B3LYP/6-31G and PBE0/cc-pVQZ levels of theory.

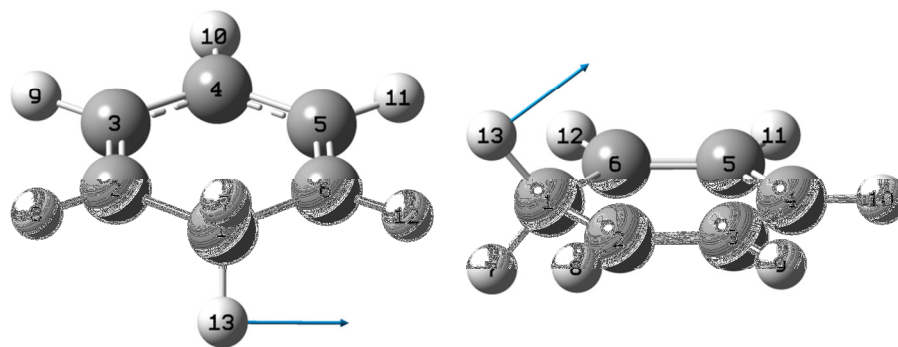


Figure 10. (Left) in plane bending and (Right) out of plane bending motions of the vibrationally isolated muon.

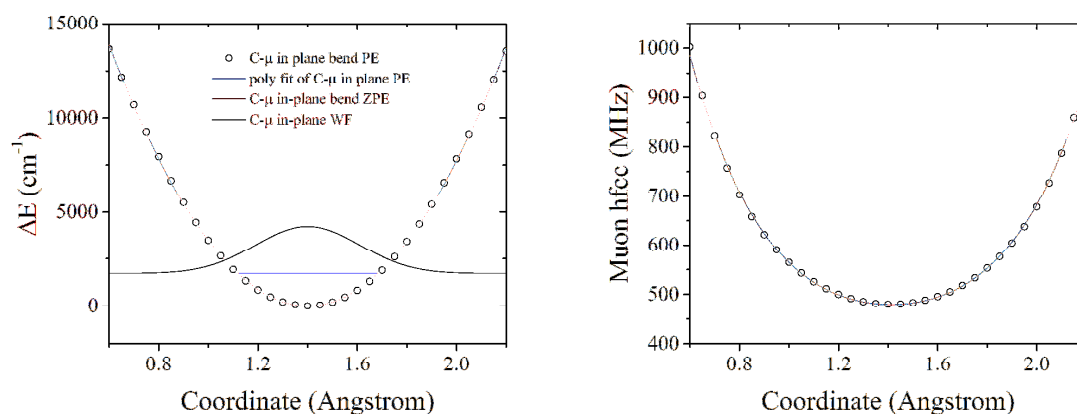


Figure 11. (Left) PES, and (right) muon hfcc as a function of the in-plane bending motion, simulated for the C_6H_7 radical using the uB3LYP/EPR-III model chemistry. Bending motion reproduced through displacement of H from a ghost atom.

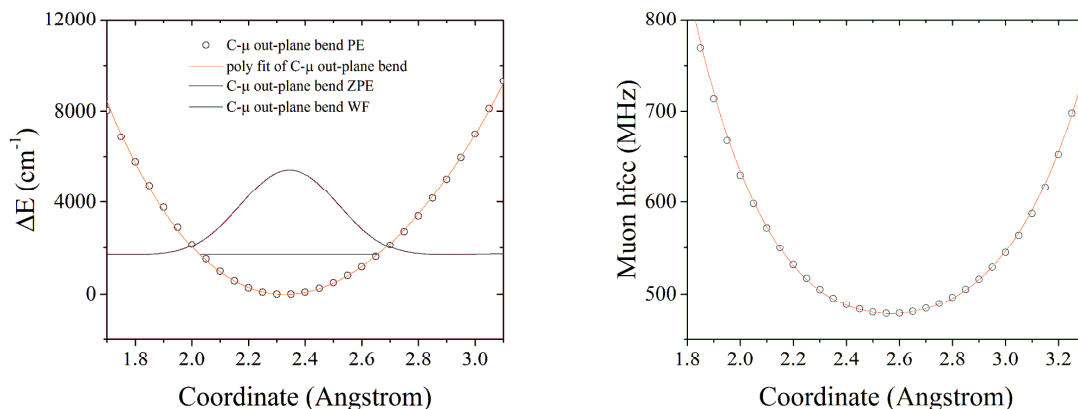


Figure 12. (Left) PES, and (right) muon hfcc as a function of the out-of-plane bending motion, simulated for the C_6H_7 radical using the $uB3LYP/EPR-III$ model chemistry. Bending motion reproduced through displacement of H from a ghost atom.

	$A_{\mu 0}$ (MHz)	Quantum Factor	A_{μ} ZPE corrected (MHz)
B3LYP/6-31G	480.41	1.041	500.06
B3LYP/6-311++G**	444.63	1.041	462.91
B3LYP/cc-pVQZ	458.55	1.041	477.46
B3LYP/EPR-II	478.72	1.041	498.81
B3LYP/EPR-III	479.71	1.041	499.51
PBEO/EPR-III	462.73	1.039	480.56
PBEO/cc-pVQZ	442.56	1.038	459.59

Table 5: Comparison of zero-point vibrationally corrected muon hfcc's for the C- μ in-plane bending mode, using a combination of functionals and basis sets. In each case the structure was initially optimised at the $B3LYP/EPR-III$ level of theory.

	$A_{\mu 0}$ (MHz)	Quantum Factor	A_{μ} ZPE corrected (MHz)
B3LYP/6-31G	483.22	1.023	493.31
B3LYP/6-311++G**	445.53	1.027	456.66
B3LYP/cc-pVQZ	458.45	1.027	470.96
B3LYP/EPR-II	478.64	1.028	491.90
B3LYP/EPR-III	479.62	1.027	492.66
PBEO/EPR-III	462.63	1.025	474.25
PBEO/cc-pVQZ	445.14	1.022	454.78

Table 6: Comparison of zero-point vibrationally corrected muon hfcc's for the C- μ out-of-plane bending mode, using a combination of functionals and basis sets. In each case the structure was initially optimised at the $B3LYP/EPR-III$ level of theory.

2.3.3 Averaging vibrational contributions for comparison with experimental data

An overall ZPE corrected hfcc, A_{TOT} can be calculated by assigning a fractional weighting to the stretching and bending contributions. Here, this was done using the vibrational frequency according to equations 17 and 18.

$$A_{TOT} = \sum_{i=1}^N f_i A_{ZPE(i)} \quad (17)$$

where A_i is the ZPE vibrationally averaged hfcc and f_i is the fractional weighting for vibrational normal modes considered

$$f_i = \frac{v_i}{\sum_{i=1}^N v_i} \quad (18)$$

where v is the vibrational frequency of each of the vibrational normal modes considered.

A_μ ZPE corrected (MHz)	
Exp.	553(2)
B3LYP/6-31G	539.66
B3LYP/6-311++G**	504.44
B3LYP/cc-pVQZ	520.58
B3LYP/EPR-II	543.12
B3LYP/EPR-III	540.17
PBEO/EPR-III	523.77
PBEO/cc-pVQZ	501.45

Table 7: Comparison of the overall ZPE corrected muon hfcc's with the experimental value obtained by extrapolating to zero K [35].

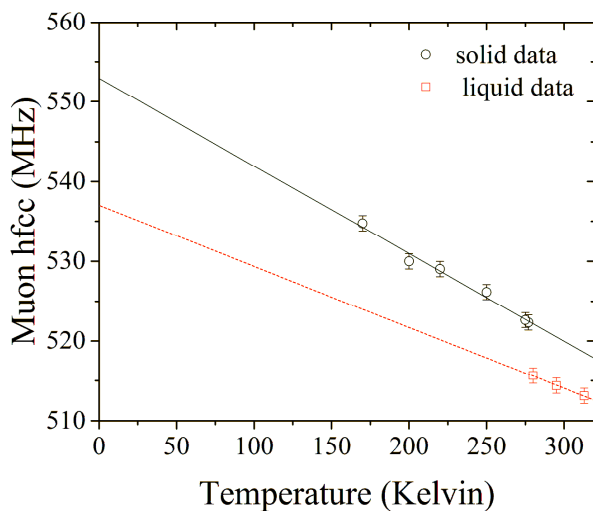


Figure 13. A_μ temperature dependence for the $[C_6H_6\mu]^\bullet$ radical, using data compiled from [35].

The overall averages (Table 7) are compared to the experimental data extrapolated back to $T=0$ K ($A_\mu = 553 (\pm 1.63)$ MHz) collected by Fleming *et al* [35]. Comparing DFT results for A_{TOT} to this value suggests a systematic underestimation, with the B3LYP functional in combination with the 6-31G, EPR-II, and EPR-III basis sets giving the best agreement (differences of 13.34 MHz, 9.88 MHz, and 12.83 MHz, respectively). None of the simulated A_{TOT} values are within experimental error, leading to a ~ 300 – 500 Gauss shift in the predicted Δ_1 resonance field position. Other combinations of the

B3LYP and PBEO functionals with different basis sets led to relatively large underestimations of A_{TOT} . Fortunately, there is plenty of scope for optimising the procedure. The first and most obvious modification would be the choice of model chemistry used for both the initial geometry optimisation and for subsequent calculation of the hfcc's. Improta and Barone noted that small changes in the equilibrium structure have large effects on the hfcc, and that these effects are particularly pronounced in π -character radicals, such as our current example [22]. If the planarity of the molecule is shifted, this can allow s -atomic orbital coefficients to contribute further to the singly occupied molecular orbital (SOMO), this directly affects the spin density at the nucleus. A worthwhile investigation would be to use a semi-empirical methodology to geometry optimise the structure. Any subsequent calculations of A are likely to be higher in magnitude, which could bring A_{TOT} closer to the experimental 553 MHz.

Another area for improvement is the description of the wave function, which was found to significantly affect the magnitude of both A_μ and A_k , so it is possible that results could be further improved by optimising it's description. In the muoniated cyclohexadienyl radical, and indeed for other semi-rigid molecules, a harmonic model should provide an adequate description of the wave function, an optimised version may be required to expand the applicability of the model to a greater variety of systems. There are studies which focussed specifically on simulating ground and low lying excited state vibrational wave functions, using variation-perturbation approaches [53, 54]. Other studies involving muoniated radicals have included a second-order perturbation of principle anharmonicities, and the authors claimed that this markedly improved the accuracy of the method [22].

2.3.4 Nuclear couplings

It is also important that our model accurately reproduces the magnitude of any nuclear couplings. We have already mentioned the limited data available for the H_{ipso} hfcc which was measured by Fleming *et al.* [35] (see Figure 14). Here, we use the data in the context of the nuclear coupling, and with the minimum number of points available to fit in the solid state, a value of 133.97 (\pm 0.13) MHz is obtained through extrapolation to $T = 0$ K. Similar issues exist with this extrapolation, as did for extrapolating A_u data. Here though, we have the smallest dataset possible to base such an extrapolation. We are again assuming a linear temperature dependence back to $T=0$ K, and there are issues relating to the splitting of the Δ_0 resonance below 180 K [35]. However, this is the only data we know to be available at the current time.

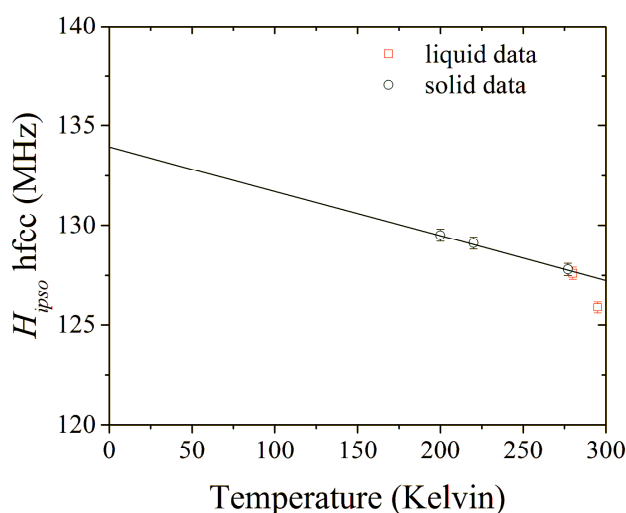


Figure 14. A_k temperature dependence for the $[C_6H_6\mu]^\bullet$ radical, using data compiled from [35].

Unlike the C- μ vibrational modes, the C-H_{ipso} modes are not vibrationally isolated. For example, the C-H_{ipso} stretching vibration also involves a translational motion of the muon, in a similar way to the C- μ out of plane bend, and the out of plane C-H_{ipso} involves ring torsions that result in the displacement of all atoms in the molecule. Gaussian does report a breakdown of the atomic displacements in Cartesian space for each molecular vibration along with associated force constants. It would be desirable to have access to a program that transforms these parameters into an input file to calculate the energy and hfcc's across the molecular displacement for any given normal mode, in a similar way to an intrinsic reaction coordinate (IRC) type calculation. To our knowledge, there is no such program that currently exists. Such a tool would also provide access to some of the more complex low energy torsional modes (see Figure 15) that are more energetically accessible at low temperatures within bulk benzene. Such an analysis may become necessary to make our model applicable to a wider variety of molecular systems. Currently though, from a practical perspective it is not possible to exactly simulate these normal modes, and we have to approximate them in isolation. Fortunately, due to the symmetry of the molecule, energy and hfcc data relating to C-H_{ipso} normal modes is the same as for C- μ modes. The difference is how we deal with the data; for C-H_{ipso}, there is no need to correct for the gyromagnetic ratio like we did for the C- μ modes. Data relating to these vibrations is reported in Tables 8, 9 and 10. As before, values for A_{k0} shown in the tables were obtained by evaluating the hfcc fitting function at the equilibrium position for each vibration. As such, small discrepancies can be observed for the values for A_{k0} reported in the tables.

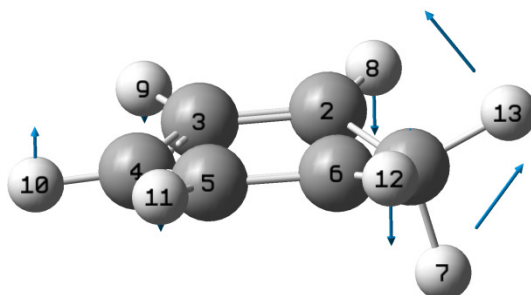


Figure 15. The lowest energy torsional mode in the muoniated cyclohexadienyl radical.

	A_{k0} (MHz)	Quantum Factor	$A_{k\text{ ipso}}$ ZPE corrected (MHz)
B3LYP/6-31G	146.81	1.036	152.03
B3LYP/EPR-II	147.46	1.037	152.94
B3LYP/EPR-III	149.00	1.036	155.09

Table 8: Comparison of zero-point vibrationally corrected muon hfcc's for the $C-H_{\text{ipso}}$ stretch, using a combination of functionals and basis sets. In each case the structure was initially optimised at the B3LYP/EPR-III level of theory.

	A_{k0} (MHz)	Quantum Factor	$A_{k\text{ ipso}}$ ZPE corrected (MHz)
B3LYP/6-31G	150.91	1.041	157.09
B3LYP/EPR-II	150.39	1.042	156.70
B3LYP/EPR-III	150.70	1.041	156.91

Table 9: Comparison of zero-point vibrationally corrected muon hfcc's for the $C-H_{\text{ipso}}$ in-plane bending mode, using a combination of functionals and basis sets. In each case the structure was initially optimised at the B3LYP/EPR-III level of theory.

	A_{k0} (MHz)	Quantum Factor	$A_{k\text{ ipso}}$ ZPE corrected (MHz)
B3LYP/6-31G	151.80	1.023	155.28
B3LYP/EPR-II	150.36	1.028	154.53
B3LYP/EPR-III	150.67	1.027	154.76

Table 10: Comparison of zero-point vibrationally corrected muon hfcc's for the $C-H_{\text{ipso}}$ out-of-plane bending mode, using a combination of functionals and basis sets. In each case the structure was initially optimised at the B3LYP/EPR-III level of theory.

Contributions from the stretching and bending modes are accounted for using equations 17 and 18; results are shown in Table 11.

	$A_{k\text{ ipso}}$ ZPE corrected (MHz)
Exp.	134 (2)
B3LYP/6-31G	154.18
B3LYP/EPR-II	154.70
B3LYP/EPR-III	155.48

Table 11: Comparison of the overall ZPE corrected H_{ipso} hfcc's with the experimental value obtained by extrapolating A_p data to zero K [35].

$A_{k\text{ TOT}}$ for the I_{pso} proton is systematically overestimated by $\sim 14\%$ for all selected methods. Practically, if the simulated data was the only information known about A_{μ} and A_k before starting an ALC type experiment, the hunt for the Δ_1 resonance would start ~ 1200 Gauss away from the resonance. Clearly this isn't good enough to be considered useful. Starting with an overall value for A_{k0} which is closer to the experimental value of 134 MHz would go some way to improving the accuracy of the method.

3 Conclusions

3.1 Outcome of the study of the cyclohexadienyl radical

A common danger with this type of study is to evaluate a property of a system using lots of different functionals/basis sets, and stop once a match is found with the experimental value. In such instances, the match is often coincidental, due to a cancellation of errors. The result is a model that gives a good match for the prototype system, but fails when applied to other more complicated systems. The simple methodology developed in section 2.3 can predict the magnitudes of A_μ in the muoniated cyclohexadienyl radical to a reasonable level of accuracy when using the B3LYP functional in combination with the well-known 6-31G, EPR-II, or EPR-III basis sets, giving a systematic underestimation of $\sim 2\%$. Results for the H_{ipso} are less promising, with a systematic overestimation of A_k by $\sim 14\%$ by all methods tested. In its current state, any of these selected levels of theory could be used to identifying A_μ and locate Δ_1 resonances in ALC type experiments. However, further development is required in order for the technique to be considered useful for predicting A_k and locating Δ_0 ALC resonances.

The procedure used to ZPE correct the muon and nuclear hfcc is as follows:

1. Calculate the PES for a static bond displacement (stretch, bend, torsional) and fit the energy vs. static displacement with an appropriate function
2. Determine the ZPE for the muoniated species
3. Simulate the wave function for the ZPE level
4. Normalise the square of the wave function and sum over all values evaluated
5. Calculate the hfcc for each displacement value, fit with an appropriate function and evaluate at the same values as the wave function
6. Calculate the product of the normalised square of the wave function with corresponding values for A_μ
7. Calculate the ratio of each of the above products with the equilibrium hfcc and sum the results
8. Calculate the ratio of the above summed value with the sum of the normalised square of the wave function to obtain the QF
9. Repeat for other modes of vibration (bend, torsional) and average
10. Combine the QF for all modes to give an overall QF and multiply by A_0 to obtain the ZPE averaged hfcc

3.2 Recommendations for further work

Although, on the face of it, the results we have presented are less than perfect, there is plenty of scope to optimise the methodology. With a little development, there is certainly potential for this to be a valuable tool for the muon user community. In particular, there are two areas which if modified would improve the accuracy of the method. Firstly, the overall value for $A_{\mu 0}$ (for the stretching and bending vibrations) should be as close to the experimental 426 MHz as possible. An alternative level of theory, such as the semi-empirical PM3 method for the initial geometry optimisation could provide a better starting structure on which to perform the averaging procedure. Secondly, in order to simulate the muon and proton couplings with any real accuracy, the overall QF should be close to the experimentally determined value of 1.3.

Once the method has been optimised, it can be properly benchmarked. However, further experimental data are required for the low temperature region of the muoniated cyclohexadienyl radical in order to confirm the assumed linear temperature dependence down to $T=0$ K. The next step would be to test the methodology on a similar radical system with known hfcc temperature dependence data. Unfortunately, we are not aware of any low temperature dependence data for muon and proton hfcc's having been published for any similar muoniated radical systems. Therefore, further down the line, we recommend extending the experimental dataset – additional TF and LF-ALC studies on a similar set of molecules. If the model doesn't hold true on the extended experimental dataset, there is merit for including some of the low energy torsional modes into the averaging procedure, and including the effects of neighbouring benzene molecules. For this, however, programs like CASTEP (using plane waves) or CRYSTAL (using Gaussian type orbitals) hold the key, these periodic potential DFT codes are much better suited for investigating how the lattice might affect the hfcc.

We anticipate this methodology becoming very time consuming for more complicated systems than our benzene prototype, particularly in linear systems which are more torsionally active. However, automation offers the potential of reducing this rather laborious task into something which could be managed by a novice user. As computing power continues to grow over the coming years, it is not out of the question to imagine a ZPE average over all $3N-6$ vibrational modes in fairly complex radical systems to be done in a routine manner by a desktop machine in the muon instrument cabin.

Note Added in Proof

Since completing this programme of work, we have discovered that an alternative approach of taking a product of the QF s for different muon zero point modes produces a much better value for the overall QF in comparison with the weighted average method suggested in the previous section. For the calculations reported here, averaged over the various models, this method gives the value $QF = 1.220(8) \times 1.040(1) \times 1.026(2) = 1.30(1)$, in perfect agreement with experiment; it is notable that the estimate of QF does not depend significantly on the model used. Thus the main problem left to address is the DFT overestimate of $A_{\mu 0}$ shown in Table 11. It seems here that the estimate of the molecular structure provided by DFT is not reliable enough for accurate estimation of absolute hfcc. However, semi-empirical methods can easily provide more reliable structures and a hybrid method [55,56,57] using PM3 for the molecular geometry and DFT for the electronic spin distribution looks very promising in this regard, giving a value of 430 MHz for $A_{\mu 0}$ at the B3LYP/cc-pVDZ level with an overall QF value of 1.30, so that $A_{\mu} = 559$ MHz, all these values being in excellent agreement with experiment. This method is now being applied to a range of systems currently being investigated by μ SR (including an extended temperature study of the cyclohexadienyl radical) and a full report will follow in due course [57].

4 Appendix

```
%chk=H.chk  
%mem=1GB  
%nprocshared=2  
# opt freq uB3LYP/6-31G
```

Geometry optimisation and frequency calculation of muoniated cyclohexadienyl radical

```
0 2  
C      0.00000000  0.00000000  1.35870848  
C      0.00000000  1.20809735  0.66121314  
C      0.00000000  1.20809735 -0.73377752  
C      0.00000000 -0.00000000 -1.43127286  
C      0.00000000 -1.20809735 -0.73377752  
C      0.00000000 -1.20809735  0.66121314  
H      0.86313355 -0.00000000  1.99108533  
H      0.00000000  2.16038781  1.21101830  
H      0.00000000  2.16038781 -1.28358268  
H      0.00000000 -0.00000000 -2.53088316  
H      0.00000000 -2.16038781 -1.28358268  
H      0.00000000 -2.16038781  1.21101830  
H     -0.86313355 -0.00000000  1.99108533
```

5 References

-
- [1] R.G. Parr and W. Yang, *Density Functional Theory of Atoms and Molecules*, Oxford Science Publications, 1989.
- [2] W. Koch, M.C. Holthausen, *A Chemist's Guide to Density Functional Theory*, 2nd Edition, Wiley, 2001.
- [3] P. Hohenberg and W. Kohn, *Phys. Rev.*, 1964, 136, B864–B871.
- [4] P. Hohenberg and W. Kohn, *Phys. Rev.*, 1965, 140, A1133–A1138.
- [5] W. Kohn and L.J. Sham, *Phys. Rev.*, 1965, 140, 1133.
- [6] A.J. Cohen, P. Mori-Sanchez, W. Yang, *Science*, 2008, 321 (5890), 792-794.
- [7] P. E. Blöchl, *Phys. Rev. B*, 1994, 50, 17953.
- [8] J. C. Slater, *Phys. Rev.*, 1930, 36, 57–64.
- [9] S. F. Boys, *Proc. R. Soc.*, 1950, 200, 542–554.
- [10] G. Frenking *et al.*, *Rev. Comp Chem.*, 1996, 8, ed. K. B. Lipkowitz and D. B. Boyd, 63–143.
- [11] T. Cundari, M. T. Benson, M. L. Lutz and S. O. Sommerer, *Rev. Comp Chem.*, 1996, 8, ed. K. B. Lipkowitz and D. B. Boyd, 145–202.
- [12] G. H. Hanson and L. J. Berliner, Springer-Verlag New York Inc., 2009.
- [13] M. J. Frisch *et al.*, *Gaussian 03*, Revision E.02, Gaussian, Inc., Wallingford, CT, 2004.
- [14] <http://cms.mpi.univie.ac.at/marsweb/>.
- [15] P. Giannozzi *et al.*, *Journal of Physics: Condensed Matter*, 2009, 21, 395502–395520.
- [16] M. W. Schmidt *et al.*, *J. Comput. Chem.*, 1993, 14, 1347–1363.
- [17] G. te Velde *et al.*, *J. Comput. Chem.*, 2001, 22, 931–967.
- [18] F. Neese, *Wiley Interdisciplinary Reviews: Computational Molecular Science*, 2012, 2, 73–78.
- [19] J. J. Mortensen, L. B. Hansen, and K. W. Jacobsen, *Physical Review B*, 2005, Vol. **71**, 035109.
- [20] S.J. Clark *et al.*, *Zeitschrift fuer Kristallographie*, 2005, 220 (5-6), 567-570.
- [21] <http://www.scarf.rl.ac.uk/>
- [22] R. Improta and V. Barone, *Chem. Rev.*, 2004, 104, 1231–1253.
- [23] D. C. Walker, *Muon and Muonium Chemistry*, Cambridge University Press, 1983.
- [24] E. Roduner, *Chem. Soc. Rev.*, 1993, 22, 337–346.

-
- [25] S.J. Blundell, *Chem. Rev.*, 2004, 104, 5717
- [26] E. Roduner. Aspects of muon chemistry. Proceedings of the 51st Scottish Universities Summer School in Physics, 1998.
- [27] Nuccio *et al.*, *J. Phys. D: Appl. Phys.*, 2014, 47, 473001.
- [28] R.F. Kiefl *et al.*, *Phys. Rev. Lett.*, 1984, 53, 90.
- [29] K. S. Yang, B. Hudson, *J. Phys. Chem.*, 2010, 114, 12283–12290.
- [30] V. Barone and A. Polimeno, *Phys. Chem. Chem. Phys.*, 2006, 8, 4609.
- [31] E.D. Hedegard, J. Kongsted, and S.P.A. Sauer, *J. Chem. Theory Comput.*, 2011, 7, 4077–4087.
- [32] R. Batra *et al.*, *J. Phys. Chem.*, 1996, 100, 18371-18379.
- [33] B.S. Hudson and S.K. Chafetz, *Molecules*, 2013, 18, 4906-4916.
- [34] E. Roduner, G. A. Brinkman and P.W. Louwrier, *Chem. Phys.*, 1982, 73, 117–130.
- [35] D. G. Fleming *et al.*, *J. Phys. Chem. C*, 2011, 115, 11177–11191.
- [36] D. Yu *et al.*, *J. Chem. Phys.*, 1990, 142, 229–236.
- [37] J. Tao, J. P. Perdew, V. N. Staroverov and G. E. Scuseria, *Phys. Rev. Lett.*, 2003, 91, 146401.
- [38] A. D. Becke, *J. Chem. Phys.*, 1993, 98, 5648–5652.
- [39] J. P. Perdew, K. Burke and M. Ernzerhof, *Phys. Rev. Lett.*, 1996, 77, 3865–3868.
- [40] C. Adamo and V. Barone, *J. Chem. Phys.*, 1999, 110, 6158–6169.
- [41] V. Barone, ed. D. P. Chong, World Scientific Publ. Co., 1996.
- [42] P. W. Percival, M. J. Ramos and B. C. Webstar, *Chem. Phys.*, 1982, 67, 275–285.
- [43] E. Roduner and I. D. Reid, *Israel J. Chem.*, 1989, 29, 3–11.
- [44] Y. K. Chen, D. G. Fleming and Y. A. Wang, *J. Phys. Chem. A*, 2011, 115, 2765–2777.
- [45] A. Lopes De Magalhaes M.J. Ramos, *Chem. Phys. Lett.*, 1990, 165 (6), 528.
- [46] M.I.J. Probert and A.J. Fisher, *J. Phys.: Condens. Matter*, 1997, 9, 3241–3257.
- [47] I. McKenzie, *J. Phys. Chem. A*, 2010, 114, 12759–12763.
- [48] I. McKenzie *et al.*, *Phys. Chem. Chem. Phys.*, 2010, 12, 9900-9908.
- [49] I. McKenzie, R. Scheurermann and K. Sedlak., *J. Phys. Chem. A*, 2012, 116, 7765–7772.
- [50] F. Pratt, unpublished.
- [51] P.W. Morse, *Phys. Rev.*, 1929, 34, 57.
- [52] H. Wei, *Phys. Rev. A* 42 (1990) 2524.

[53] P.-O Astrand, K. Ruud, P.R. Taylor, J. Chem. Phys., 2000, 112, 2655.

[54] K. Ruud, P.-O. Astrand, P.R. Taylor, J. Chem. Phys., 2000, 112, 2668.

[55] F.L. Pratt, 'Simulation of Molecular ALC Spectra using Density Functional Theory', ISIS Muon User Meeting, 17th Sept 2012

[56] F.L. Pratt, 'ALC Spectra of Molecular Solids: Effects of Multiple Sites, Crystalline Environment and Quantum Delocalisation', 13th International Conference on Muon Spin Rotation, Relaxation and Resonance, Grindelwald 1st-6th June 2014 (Special Session on Muon Site and Related Issues)

[57] F.L. Pratt (in preparation)